

Sebastian Nau, BSc

Efficiency and Stability of Poly(indenofluorene)-based Homo- and Copolymers

MASTER THESIS

For obtaining the academic degree
Diplom-Ingenieur

Master Programme of
Technical Physics



Graz University of Technology

Supervisor:

Ao.Univ.-Prof. Dipl.-Ing. Dr.techn. Emil J. W. List
Institute of Solid State Physics

in cooperation with:
NanoTecCenter Weiz Forschungsgesellschaft mbH

Graz, April 2011

Deutsche Fassung:
Beschluss der Curricula-Kommission für Bachelor-, Master- und Diplomstudien vom 10.11.2008
Genehmigung des Senates am 1.12.2008

EIDESSTÄTTLICHE ERKLÄRUNG

Ich erkläre an Eides statt, dass ich die vorliegende Arbeit selbstständig verfasst, andere als die angegebenen Quellen/Hilfsmittel nicht benutzt, und die den benutzten Quellen wörtlich und inhaltlich entnommene Stellen als solche kenntlich gemacht habe.

Graz, am

.....
(Unterschrift)

Englische Fassung:

STATUTORY DECLARATION

I declare that I have authored this thesis independently, that I have not used other than the declared sources / resources, and that I have explicitly marked all material which has been quoted either literally or by content from the used sources.

.....
date

.....
(signature)

Acknowledgement

I would like to express my sincere thanks to my supervisor Professor Emil J. W. List for making this work possible and for his constructive criticism.

I am truly thankful to Stefan Sax for his great guidance throughout this project, many helpful discussions and his friendship.

Furthermore I want to thank Roman Trattnig who taught me the basics of the fabrication process of PLEDs, Sebastian Schuh for his helping hands, Alexander Blümel for introducing me to atomic force microscopy and Cornelia Ranz for showing me how to deal with chemicals.

It is a pleasure to thank my office colleagues of the first hour, Kerstin Schmoltner and Johannes Kofler, who made this work so much easier and became good friends. I would also like to show my gratitude to the whole team of the NanoTecCenter Weiz Forschungsgesellschaft mbH. Thanks also go to Joanneum Research Materials, in particular Christian Sommer and Elke Kraker for their support.

Moreover I want to thank my lovely girlfriend Evelyn for her understanding and many valuable and encouraging words.

Lastly, but most important, I want to thank my family, especially my deceased father and my mother for her caring and support in the 26 years of my life. I know that such a backing cannot be taken for granted and I greatly appreciate that.

Thank you!

Abstract

Polymer light-emitting diodes (PLEDs) are one of the most promising applications of organic semiconductors. Among others, PLED full color displays require the three primary colors blue, green and red for proper color presentation. Green and red light emitting polymers have already been realized with the desired properties. Blue light emitting polymers, however, still suffer from their limited efficiency and stability. This work presents different approaches to investigate novel poly(indenofluorene) based homo- and copolymers with respect to the stated properties. One of the important values which determine the efficiency of light emitting materials is the photoluminescence quantum yield and an indirect method to measure this value was successfully applied here. Besides that, a detailed study of the photoluminescence related stability with respect to different influences (thermal stress under air and under argon, UV irradiation and acidic environments) was carried out. Of special interest were any interactions of the emissive polymer with poly(3,4-ethylenedioxythiophene) poly(styrenesulfonate) (PEDOT:PSS) which has an acidic character and is used in almost every efficient PLED device as injection and smoothing layer. Different influences on the components of the polymer chain were observed. Further on, the operational stability of PLED devices in oxygen and humidity containing atmospheres was investigated. The results strongly indicate static and dynamic quenching. Different single-layer and multi-layer PLED configurations were tested with respect to luminance and efficiency. The best results were obtained from anode/hole transporter/emitter/electron transporter/cathode architectures. The fabrication of such solution processed multi-layer devices is challenging, since one has to ensure that the solvent of the subsequent solution does not dissolve the layer beneath. Hence, a part of the work deals with fabrication aspects of such polymer heterostructures from solution.

Kurzfassung

Polymer-basierende Licht emittierende Dioden (PLEDs) sind eine der vielen viel versprechenden Anwendungsmöglichkeiten von organischen Halbleitern. Für eine farbtreue Bildwiedergabe benötigen u.a. PLED Displays die drei Grundfarben Blau, Grün und Rot. Rot und Grün emittierenden Materialien wurden bereits erfolgreich mit den gewünschten Eigenschaften entwickelt. Blau emittierende Polymere sind jedoch nach wie vor in ihrer Effizienz und Stabilität eingeschränkt. Diese Masterarbeit hat sich zum Ziel gesetzt, neuartige Polyindenofluoren-basierende Homo- und Copolymere im Bezug auf diese zwei Eigenschaften zu untersuchen. Die Effizienz von Polymer-basierenden Bauteilen ist unter anderem durch die Photolumineszenz-Quantenausbeute des emittierenden Materials definiert. Um diese messtechnisch zu erfassen wurde eine indirekte experimentelle Methode erfolgreich angewandt. Weiters wurde die spektrale Stabilität unter dem Einfluss von thermischem Stress, UV-Bestrahlung und sauren Medien untersucht. Von besonderem Interesse waren Interaktionen mit Poly-3,4-ethylendioxythiophen Polystyrensulfonat (PEDOT:PSS), da dieses Polymer in nahezu jeder effizienten PLED als Injektions- und Glättungsschicht Anwendung findet. Diese Degradationsstudien zeigten verschiedenste Einwirkungen auf die Bestandteile der Polymerkette. Weiters wurde die Stabilität von PLEDs, die in einer künstlichen Sauerstoffhaltigen oder befeuchteten Atmosphäre betrieben wurden, untersucht. Die hier gemessenen Effekte deuten stark auf eine statische oder dynamische Fluoreszenzlöschung hin. Ebenso wurden verschiedene Ein- und Mehrschicht PLED Strukturen bezogen auf ihre Helligkeit und Effizienz getestet. Dabei wurden mit Lochtransporter/Polymer/Elektronentransporter - Mehrschichtsystemen die besten Ergebnisse erzielt. Die Herstellung solcher Mehrschichtsysteme aus Lösung ist problematisch da das Lösungsmittel der aufzubringenden Schicht oft die darunterliegende Schicht wieder an- oder auflöst. Ein Teil dieser Arbeit beschäftigt sich daher auch mit fabrikationsbezogenen Aspekten von polymeren Mehrschichtsystemen.

Table of contents

Acknowledgement	II
Abstract.....	III
Kurzfassung	IV
Table of contents	V
List of abbreviations	VII
1 Introduction and motivation.....	8
2 Light emitting organic semiconductors.....	9
2.1 Fundamentals	9
2.2 Design and properties of poly(para-phenylene)-type blue emitting polymers.....	11
2.3 Fundamental excitations	13
2.4 Photoexcitation, luminescence and non-radiative deactivation	14
2.5 Photoluminescence quantum yield	17
2.5.1 Limiting factors – Quenching	17
2.5.2 Molecular oxygen – an important quencher	20
3 Polymer light emitting diodes	23
3.1 Working principle	23
3.2 Electroluminescence quantum yield	26
3.3 Device degradation and related processes	27
3.3.1 EL quantum yield reducing factors.....	28
3.3.2 Organic / Cathode interface	28
3.3.3 Anode / Organic interface.....	29
3.3.4 Bulk material	29
4 Experimental methodology	31
4.1 Solution and thin film preparation	31
4.2 Layer thickness measurements	31
4.3 Optical absorbance measurements	32
4.4 Photoluminescence measurements.....	32
4.5 Calibration of a spectrofluorophotometer	33
4.6 Photoluminescence quantum yield (for solutions).....	36
4.7 PLED device preparation	40
5 Photophysical characterization of poly(indenofluorene)-based polymers	42
5.1 Emitter materials	42
5.2 Hole transport material	46
5.2.1 Photophysical properties of <i>htlPIF</i>	46

5.2.2	Fabrication of multi-layer structures	47
5.3	Summary and discussion.....	48
6	Photoluminescence related material stability.....	50
6.1	Stability with respect to thermal stress	50
6.1.1	homoPIF	50
6.1.2	coPIF-1	52
6.1.3	coPIF-2	53
6.2	Stability with respect to UV irradiation.....	54
6.3	Stability with respect to acidic environments	57
6.3.1	PIF / PEDOT:PSS double layers	57
6.3.2	PIF / Trifluoroacetic blends	59
6.3.3	PIF / HCl interactions	60
6.4	Summary and discussion.....	61
7	Operational stability of PLED devices.....	64
7.1	Adopted PLED design and experimental methodology.....	64
7.2	Stability of homoPIF.....	65
7.3	Stability of coPIF-1	66
7.4	Stability of coPIF-2.....	67
7.5	Summary and discussion.....	69
8	PLED device optimization with respect to their efficiency	71
8.1	htlPIF and TPBi-only device	72
8.2	PLEDs based on homoPIF.....	73
8.2.1	ITO/PEDOT:PSS/150 nm homoPIF/Ca/Al	73
8.2.2	ITO/PEDOT:PSS/htlPIF/homoPIF/TPBi/Ca/Al.....	75
8.2.3	ITO/PEDOT:PSS/htlPIF+homoPIF/TPBi/Ca/Al	76
8.2.4	Summary and discussion	77
8.3	PLEDs based on coPIF-1	79
8.3.1	ITO/PEDOT:PSS/150 nm coPIF-1/Ca/Al	79
8.3.2	ITO/PEDOT:PSS/htlPIF/coPIF-1/TPBi/Ca/Al.....	80
8.3.3	ITO/PEDOT:PSS/htlPIF+coPIF-1/TPBi/Ca/Al	81
8.3.4	Summary and discussion	81
8.4	PLEDs based on coPIF-2	84
8.4.1	ITO/PEDOT:PSS/150 nm coPIF-2/Ca/Al	84
8.4.2	ITO/PEDOT:PSS/htlPIF/coPIF-2/TPBi/Ca/Al.....	84
8.4.3	ITO/PEDOT:PSS/htlPIF+coPIF-2/TPBi/Ca/Al	85
8.4.4	Summary and discussion	86
9	Conclusion	88
	Bibliography	90

List of abbreviations

AFM	Atomic force microscopy / Atomic force microscope
BAM	Federal institute of materials and testing
CIE	Commission internationale de l'éclairage - International commission on illumination
EL	Electroluminescence
ELQE	Electroluminescence quantum efficiency
ETL	Electron transport layer
HCl	Hydrochloric acid
HOMO	Highest occupied molecular orbital
HTL	Hole transport layer
HV	High vacuum
ITO	Indium tin oxide
LUMO	Lowest unoccupied molecular orbital
MO	Molecular orbital
OSC	Organic semiconductor
PEDOT:PSS	Poly(3,4-ethylenedioxythiophene) poly(styrenesulfonate)
PIF	Poly(indenofluorene)
PL	Photoluminescence
PLED	Polymer light emitting diode
PLQY	Photoluminescence quantum yield
PMT	Photomultiplier tube
PPP	Poly(para phenylene)
PPV	Poly(phenylene vinylene)
TFA	Trifluoroacetic acid

1 Introduction and motivation

The starting point of the rapid development of organic semiconductor technology is generally assigned to the discovery of electrical conductivity in doped polyacetylene by Heeger et al. in 1977.¹ Since this, organic semiconductor technology is emerging and many different applications like organic light emitting diodes², organic photovoltaic cells³, organic field effect transistors⁴ and many others were demonstrated and already play an industrial role. However, a drawback for a cheap and efficient commercialization of organic semiconductor technology like PLED displays still is the high reactivity of the devices to oxygen and humidity. Different inorganic, organic or hybrid sealings are used to exclude these two substances, but the desired low permeabilities ($<10^{-6}$ g/m²d for water vapour and $<10^{-6}$ cm³/m² d bar for oxygen) can only be reached in demanding processes so far.^{5,6}

The scope of this work is the investigation of photophysical and electrooptical properties of novel poly(indenofluorene) based homo- and copolymers with respect to their efficiency and stability in different environments. In the following chapter 2, a short overview of the physical fundamentals of organic semiconductors and an introduction into photophysics will be given. Chapter 3 deals with the working principle of polymer light emitting diodes and device degradation related processes. An indirect method to measure the photoluminescence quantum yield (PLQY) for solutions, which is a key property of every light emitting material, will be presented in chapter 4. The experimental results are split into four chapters: Chapter 5 shows the basic photophysical properties of the novel compounds: Absorbance and photoluminescence from solutions and from thin films as well as their photoluminescence quantum yield. In addition, the cross-linking property of a hole transporting material was investigated since this is a basic requirement for the fabrication of solution processed multi-layer PLEDs. Chapter 6 presents the stability of the photoluminescence spectrum with respect to different environments (thermal stress under air and under argon atmosphere, UV irradiation, acidic environments). The influence of oxygen and humidity to the emitted light intensity of PLED devices will be shown in chapter 7. In chapter 8, the optimization of PLED architectures with respect to luminance and efficiency will be presented. Especially, a novel solution processed hole transport layer will be applied.

2 Light emitting organic semiconductors

The following sections 2.1 and 2.2 deal with fundamentals of organic semiconductors and about the basic design of blue emitting polymers. The sections 2.3 - 2.5 outline radiative and non-radiative processes in organic semiconductors and the influences of impurities and the presence of other molecular species to them.

2.1 Fundamentals

The semiconducting properties of various organic compounds arise from the special structure of this class of materials. The main component of an organic semiconductor is carbon. Carbon is the 4th main group element with 6 electrons and hence a $1s^2 2s^2 2p^2$ ground state configuration. This configuration allows only two electrons to form bonds, which is in strong contrast to experimental observations where four equal binding orbitals were found. In 1931, Linus Pauling⁷ formulated the theory of orbital hybridization and explained this discrepancy: Parts of the binding energy are used to promote one electron from the 2s orbital to the unoccupied 2p orbital. A linear combination of the wave functions of the 2s orbital and either one, two or three 2p orbitals lead to energetically equal hybrid orbitals, correspondingly denoted as sp , sp^2 or sp^3 hybridization. Figure 2.1 presents the described formation of four sp^3 orbitals.

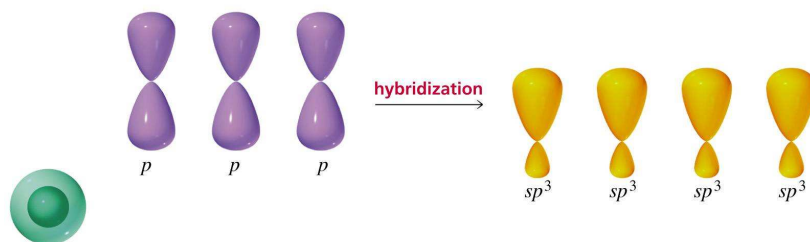


Figure 2.1: The principle of the sp^3 hybridization. Taken from [8]

The alternation of carbon double and single bonds is the foundation of organic semiconductors: This is based on a sp^2 -hybridization of the carbon atoms (Figure 2.2). Three energetically equal sp^2 orbitals form strong σ -bonds (rotation symmetric to the bond axis) with the neighboring atoms. The remaining p orbital is perpendicular oriented to

the plane of the sp^2 orbitals and forms a weaker π -bond with a neighboring p orbital of a carbon atom. The electrons in such a π -bond are strongly delocalized. Find the orbital structure of ethylene as an example for a material with a carbon double bond in figure 2.2 (right).

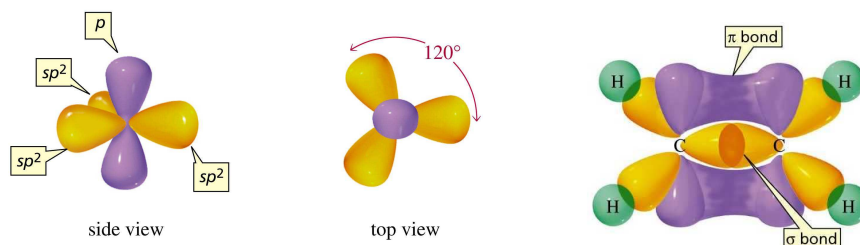


Figure 2.2: The sp^2 hybridization of carbon. From left to right: Side and top view of the orbitals of a single carbon atom. Carbon double bond in the case of ethylene, C_2H_4 . (Taken from [8] and modified)

As mentioned, the semiconducting properties of an organic compound arise from conjugation, which refers to alternating single and double bonds. However, this is just a model assumption, in fact, in a conjugated system all bonds are equal and the π -bonds form a strongly delocalized molecular orbital over the whole system. The benzene ring, C_6H_6 , is given as example in figure 2.3.

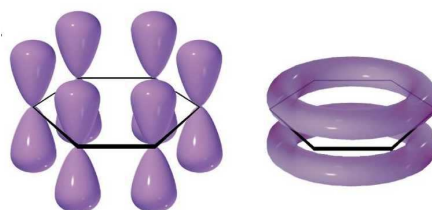


Figure 2.3: The benzene ring with localized p-orbitals (left) and with a strongly delocalized molecular orbital (right). Taken from [8].

The molecular orbital theory predicts that the two atomic orbitals which form the bond split up into a binding molecular orbital - π , and into an anti-binding molecular orbital - π^* . Pauli's exclusion rule tells that each orbital can contain two electrons and since the π -bond is lower in energy, the electrons contributed by the p-orbitals of the carbon atoms (one electron per atom) fill this band completely. The π^* -orbital remains unoccupied. If the energy gap between the bonding orbital (or highest occupied molecular orbital - HOMO) and the anti-bonding π^* -orbital (or lowest unoccupied molecular orbital - LUMO) is correspondingly small, the material can be denoted as semiconductor. The

energy of HOMO and LUMO, and thus the band gap can be tuned by structural modifications of the polymer. Since the band gap corresponds to the emission color, different emission colors can be obtained in this way.

2.2 Design and properties of poly(para-phenylene)-type blue emitting polymers

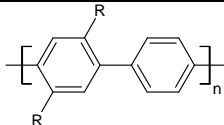
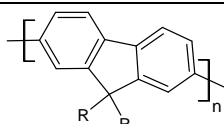
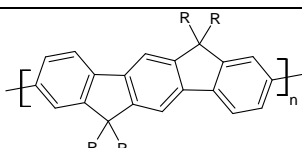
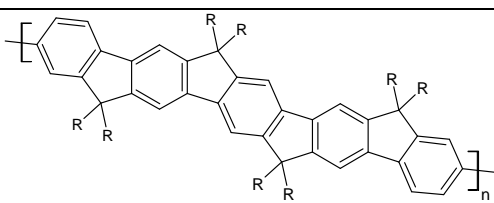
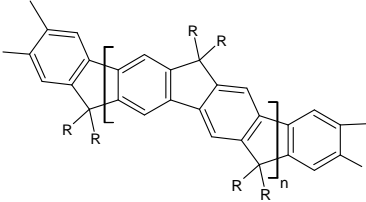
Efficient and stable blue electroluminescence emission is a basic demand for full colour light emitting devices such as displays. The human brain interprets electromagnetic radiation in the range from 435 nm (2.85 eV) to 480 nm (2.58 eV) as blue colour, thus blue emitting polymers are high band gap materials.⁹ In order to achieve bright blue emission, the band gap of the emitter has to be optimized with respect to the visual sensitivity of the human eye (Figure 2.4, black line/squares) as well as to emitted colour. It can be seen that the sensitivity for blue colour is low (<10%) compared to the sensitivity maximum at 555 nm which corresponds to a green to yellow colour. Therefore, blue emitters have to emit higher radiant intensities to create an equal brightness impression.

Poly(para-phenylene)-type (PPP-type) materials are a promising class of polymers with respect to their emission colour as well as to their efficiency. The basic PPP structure is made up of para-linked benzene rings (aryl groups) and optional side chains. Table 2.1 summarizes five PPP-type polymers with an increasing degree of aryl bridging.

Polymer **1**, a poly(para-phenylene), typically shows a single unstructured emission peak around 390 nm which is too far in a violet spectral region and hence not suitable for the human eyes colour perception.⁹

The repeating unit of the probably most famous blue emitting polymer, poly(fluorene) (**#2**), consists of two methylene bridged phenylenes. The 9-position can be substituted with different side-chains such as alkyls¹⁰, aryls¹¹ or dendritic structures¹². Its typical emission maximum appears at around 422 nm and is therefore suitable as blue emitter. However, frequently an unwanted low energy emission around 530 nm can be observed which is generally assigned to an oxidative degradation.¹³

Table 2.1: PPP-type polymers and their typical emission maxima

#	Name	Chemical structure	Typical λ_{\max}
1	Poly(para-phenylene)		390 nm
2	Poly(fluorene)		422 nm
3	Poly(indenofluorene)		428 nm
4	Poly(ladder-type pentaphenylene)		448 nm
5	Fully planarized ladder-PPP		460 nm

The polymer consisting of three aryl groups with two methylene bridges are denoted as poly(indenofluorene) (#3) - the material of interest in this work. Its synthesis was reported in 1999 by Müllen et al.¹⁴ Poly(indenofluorenes) with alkyl and aryl¹⁵ substituted side-chains were published so far, where the latter exhibits an increased resistance to oxidization. Its emission maximum is again slightly red shifted and appears around 428 nm, which comes close to the desired wavelength region for blue emitters.

A further increase in the degree of bridging and thus rigidity was achieved with poly(ladder-type pentaphenylene)¹⁶. A full aryl-substitution of every bridgehead led to the best spectral stability.¹⁷ The emission spectrum of this material shows an ideal match with the above defined desired wavelength region.

The fully planarized ladder-PPP¹⁸ (#5) is the most rigid species of PPP type materials with the lowest band gap. Its emission maximum appears around 460 nm which is already to far in the green spectral region for applications as pure blue emitter.⁹

Figure 2.4 depicts the emission spectra of poly(fluorene), poly(indenofluorene), poly(ladder-type pentaphenylene) and ladder PPP and compares it to the sensitivity of the human eye.

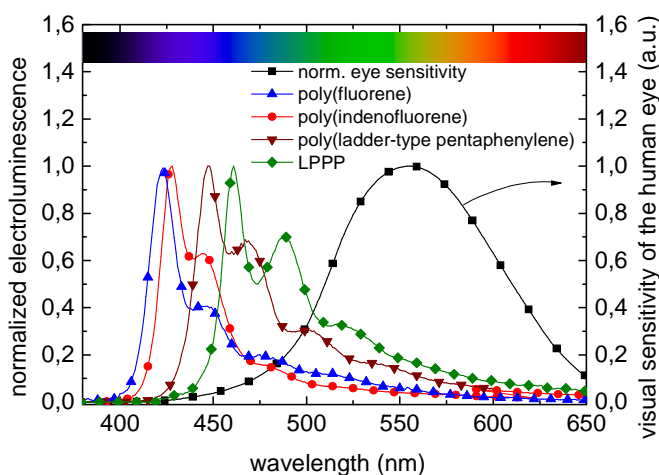


Figure 2.4: Comparison of the electroluminescence emission spectra of different PPP-type polymers to the sensitivity of the human eye.

2.3 Fundamental excitations

Polarons - charged quasiparticles

If an electron is taken away from the HOMO or is added to the LUMO, the polymer reacts to this additional charge with a structural relaxation and energetic states within the band gap are the result. In strong contrast to inorganic semiconductors, where the charge can move freely within the conduction and valence band of the crystal, polarons are strongly localized states. An additional electron in the LUMO is called negative polaron, while a missing electron (or hole) in the HOMO is called positive polaron. Correspondingly, two additional electrons or holes are denoted as negative or positive bipolarons, respectively. A scheme of these energetic states is depicted in figure 2.5.

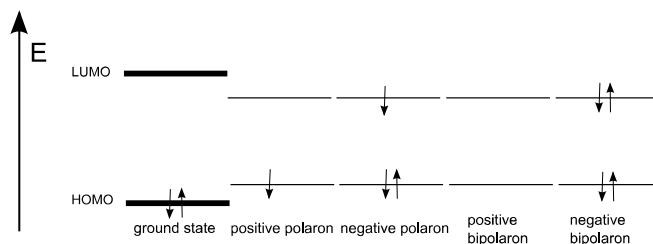


Figure 2.5: Energy levels of positive and negative polaron and bipolaron.

Excitons - neutral quasiparticles

Two electrostatically bound polarons of opposite charge are called exciton. Those excitons are strongly localized and weakly bound (~ 0.3 eV in poly(fluorene)¹⁹) and can thus be denoted as Frenkel excitons.²⁰ Predicted by basic quantum mechanics, two spin-1/2 particles (i.e. the excited electron from the LUMO and the hole from the HOMO) can form one out of four spin wave functions:

$$\text{Singlet state} \quad |\Psi_s\rangle = \frac{1}{\sqrt{2}} (|\uparrow\downarrow\rangle - |\downarrow\uparrow\rangle)$$

$$\text{Triplet states} \quad |\Psi_t\rangle = |\uparrow\uparrow\rangle \quad |\Psi_t\rangle = \frac{1}{\sqrt{2}} (|\uparrow\downarrow\rangle + |\downarrow\uparrow\rangle) \quad |\Psi_t\rangle = |\downarrow\downarrow\rangle$$

The upper wave function exhibits a total spin of 0 and is denoted as singlet state, whereas the remaining three wave functions are triplet states with a total spin of 1.

Transport of polarons in organic semiconductors

In a microscopic picture the transport of charge within an organic semiconductor can be described by a phonon assisted tunneling process. The charges hop from their localized state to other localized states on adjacent polymer units, driven by lattice vibrations. The charge transfer rate is described by the Marcus theory²¹.

2.4 Photoexcitation, luminescence and non-radiative deactivation

The fundamental radiative and non-radiative processes which an organic semiconductor can undergo are based on its electronic and vibrational states. Typically these energy

levels and transitions between these states are visualized in a Jablonski diagram (Figure 2.6).

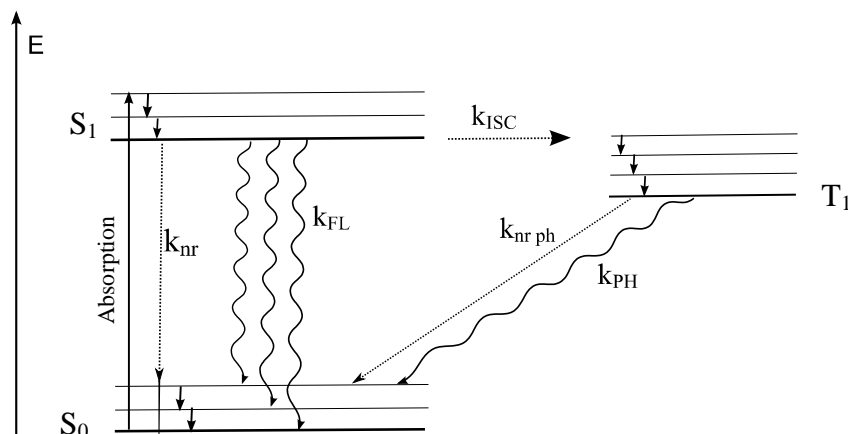


Figure 2.6: Jablonski diagram of an arbitrary organic semiconductor. The horizontal lines show the electronic end vibrational energy levels. The arrows show the possible radiative and non-radiative transitions between the participating energy levels.

The electronic ground state of an organic semiconductor is a singlet state – S_0 with several vibrational modes. The excited states are either singlet states or triplet states, while the first singlet and triplet state is depicted in the diagram. Correspondingly, each of the excited states have several vibrational energy levels.

During the absorption process, an electron from the HOMO is excited to the LUMO and forms an exciton with the remaining hole in the HOMO. Due to conservation of spin in case of electromagnetic dipole transitions, the absorption of light always leads to the formation singlet excitons. The physics of this process can be described by the Franck-Condon principle: The transition typically occurs in a very short period of time ($<10^{-15}$ s) and the nuclei of the atoms are not able to react with a displacement in this short time due to their inertia. Since the potential minima of the electronic ground and excited states are shifted to each other, this transition often ends up in an excited vibrational state of the excited singlet state according to the integral overlap of the vibrational wave functions. This principle is illustrated in figure 2.7.

However, Kasha's rule²² predicts that the electron quickly relaxes to the vibrational ground state of the excited electronic state (internal conversion). Several competing processes are now possible:

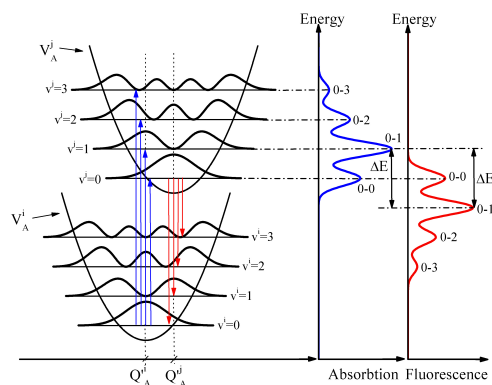


Figure 2.7: Frank-Condon Principle: Only transitions which do not change the nuclear coordinates are allowed.

Fluorescence: k_{FL} is the rate of radiative recombination of singlet excitons. This transition is called fluorescence and usually ends up in a higher vibrational state of the electronic ground state but again relaxes quickly to the lowest lying vibrational state (according to Franck-Condon principle, Figure 2.7). Hence, the absorbed photons are typically higher in energy than the emitted ones. The energy difference between the absorption and emission maximum is called Stokes-shift. Theoretically, the emission spectrum is the exact mirror image of the absorption spectrum, but lower in energy. However, torsional degrees of freedom of the phenyl rings to each other can lead to a breakdown of this principle.²³ The absorption spectrum is mostly unstructured for polymers like poly(indenofluorene), while the emission spectrum shows distinct vibrational features. The more rigid a polymer chain is, the more the mirror image rule is valid.

Non-radiative recombination: k_{nr} is the rate of non-radiative recombinations of singlet excitons, $k_{nr\text{ ph}}$ is the rate of non-radiative recombination of the triplet state, respectively. Such non-radiative recombinations are caused by structural defects, chemical defects and impurities. The energy of the excited state is dissipated as heat.

Intersystem crossing: k_{ISC} is the rate of an actually forbidden transition because it populates a triplet level which implies a spin conversion. It is dependent on different factors, such as temperature²⁴ and chemical surroundings. In molecular systems consisting of atoms with low mass numbers, spin-orbit coupling (Russel-Saunders or LS – coupling) is low and the total spin is conserved. If the molecule or polymer contains any atoms with higher masses (e.g. transition metal complexes), spin-orbit coupling gets

significant (jj-coupling). The total spin is no conserved quantity anymore and the strong forbiddenness of a spin conversion is weakened.

Phosphorescence: k_{ph} , is the rate of radiative recombinations of the excited triplet state. This process is commonly denoted as phosphorescence and ends up in the singlet ground state. On the basis of a purely electronic transition, the triplet \rightarrow singlet conversion is again strictly spin forbidden. However, the long-lasting excitation of triplet states gives rise to substantial electron-core interactions and the nature of the excited state can now be described as a singlet/triplet superposition. This opens the pathway for phosphorescence. Thus, triplet states typically have a long radiative lifetime in the range of microseconds to seconds which is several orders of magnitude higher than that of fluorescence. Consequently, only very limited phosphorescence can be found from molecules or polymers consisting of hydrocarbons (or other low mass atoms) solely. However, strong phosphorescence can be observed for heavy atoms containing materials such as organometallic complexes due to enhanced spin-orbit coupling.

2.5 Photoluminescence quantum yield

The photoluminescence quantum yield is a key property of every light emitting material. It is defined by the ratio of the emitted photons to the absorbed photons. An equal expression is the rate of radiative recombinations over the overall decay rate,

$$\Phi = \frac{\text{photons emitted}}{\text{photons absorbed}} = \frac{k_r}{k_r + k_{nr}}. \quad (2.1)$$

Φ ... Photoluminescence quantum yield; k_r ... Rate of radiative decay; k_{nr} ... Rate of non-radiative decay;

2.5.1 Limiting factors – Quenching

Quenching denotes any process that reduces the basic fluorescence or phosphorescence intensity of a material.⁴³ This section mainly deals with three of them: dynamic quenching, static quenching and quenching on chemical defects. Many other interactions are possible including field induced exciton dissociation²⁵, singlet-triplet annihilation²⁶ and quenching by polarons²⁷. Due to its special electronic configuration, molecular oxygen

is one of the most important quenchers. A detailed discussion about oxygen and the related quenching mechanisms will be given in subsection 2.5.2.

Dynamic quenching

Dynamic quenching is related to a diffusive encounter between an excited polymer and a quencher. The rate of quenching competes with the rate of radiative decay k_r and with the rate of non-radiative deactivation k_{nr} . Equation (2.1) has to be adapted to

$$\Phi_Q = \frac{k_r}{k_r + k_{nr} + k_q \cdot [Q]}. \quad (2.2)$$

Φ_Q ... PLQY in presence of a quencher with concentration Q ; k_r ... Rate of radiative decay; k_{nr} ... Rate of non-radiative decay; k_q ... Quenching rate;

The ratio Φ/Φ_Q leads to the Stern-Volmer equation,

$$\frac{\Phi}{\Phi_Q} = \frac{I}{I_Q} = \frac{\tau}{\tau_Q} = \frac{\frac{k_r}{k_r + k_{nr}}}{\frac{k_r}{k_r + k_{nr} + k_q \cdot [Q]}} = \frac{\frac{1}{\tau}}{\frac{1}{\tau} + k_q \cdot [Q]} = 1 + \tau \cdot k_q \cdot [Q]. \quad (2.3)$$

Φ ... PLQY in absence of quenchers; Φ_Q ... PLQY in presence of a quencher with concentration Q ; I ... Luminescence intensity in absence of a quencher; I_Q ... Luminescence intensity in presence of a quencher with concentration Q ; τ ... Excited state lifetime in absence of quenchers; τ_Q ... Excited state lifetime in presence of a quencher with concentration Q ; k_r ... Rate of radiative decay; k_{nr} ... Rate of non-radiative decay; k_q ... Quenching rate;

The Stern-Volmer equation relates the PLQY to a quencher concentration. Since the quantum yield is directly proportional to the radiative intensity and to the excited state lifetime, the Stern-Volmer equation provides also information about their behavior in presence of a quencher.

Three actual quenching processes are described in the following⁴³:

- *Enhanced intersystem-crossing*: Interactions with heavy atoms or oxygen can weaken the strong forbiddenness of a spin conversion which leads to an en-

hanced intersystem-crossing $S_1 \rightarrow T_1$. The now populated long living triplet states can now also be quenched by the same quencher.

- *Förster resonant energy transfer (FRET)*: An excited polymer (donor) and a quencher in its ground state (acceptor) are involved in this process. FRET causes a transfer of the excitation energy from the donor to the acceptor due to dipole-dipole interactions: The excited electron in the LUMO of the donor returns to the ground state whereas a ground state electron of the acceptor is lifted to the LUMO simultaneously. The energy transfer rate can be approximated by

$$k_{FRET} = \frac{1}{\tau_D} \cdot \left(\frac{R_0}{r}\right)^6. \quad (2.4)$$

k_{FRET} ... Förster energy transfer rate; τ_D ... Excited state lifetime of the donor; R_0 ... Förster radius; r ... Molecular distance between quencher and excited molecule;

The rate depends on the excited state lifetime of the donor (τ_D), the molecular distance between dye and quencher (r) and the radius of 50% energy transfer efficiency (R_0 , Förster radius). The latter is dependent of several factors including the spectral overlap of the absorption spectra of the two species. FRET is a long range (up to 10 nm) and spin conserving process. Thus, only singlet excitons are prone to Förster resonant energy transfer.

Note that in terms of quenching one is only interested in the fact that the donor returns into its ground state non-radiatively. The acceptor can dissipate its energy in heat or light. The same is also valid for the following process.

- *Dexter electron exchange*: As the name tells, this quenching process is due to the exchange of electrons between an excited polymer (donor) and the quencher (acceptor): An excited electron from the donor tunnels to the acceptor and populates an excited state. Simultaneously, an electron from the acceptors HOMO tunnels to the ground state of donor. After all, the donor is in its ground state and the acceptor in its excited state. Such a tunneling process requires an overlap of the involved orbitals and hence the Dexter electron exchange is a short distance process. The transfer rate decays exponentially with increasing molecular distance.

Dynamic quenching can be identified by plotting the excited state lifetime relation (τ/τ_0) or the luminescence intensity relation (I/I_0) over the quencher concentration which then gives a linear, non-zero slope. Increasing the sample temperature leads to decreased luminescence intensity because of enhanced diffusion and thus more encounters between excited polymers and quenchers.

Static quenching

In contrast to diffusive interactions between polymer and quencher, static quenching is related to the formation of non-emissive ground state complexes. These complexes can absorb photons (usually in another energy region than the polymer solely), but returns to the ground state without the emission of light. The excitation energy dissipates as heat.

Static quenching can also be identified by plotting the excited state lifetime relation (τ/τ_0) over the quencher concentration. Due to the fact that static quenching does not alter the lifetime of the unperturbed excited states, this lifetime ratio should be 1. Moreover, the total emitted intensity increases with higher sample temperature due to the breakup of the ground state complexes.

Quenching at chemical defects

This fluorescence limiting factor can for example be observed in polymers with photo-oxidized segments, such as carbonyl groups in PPVs.²⁸ The high electron affinity of these groups causes the electron-hole pair to dissociate into free polarons which reduces the quantum yield.²⁹ This model is supported by increased photocurrents in oxidized materials.²⁸ Quenching also occurs at structural defects such as incomplete conjugation or impurities like remaining synthesis precursors.

2.5.2 Molecular oxygen – an important quencher

The molecular orbital theory allows the description of the very unique electronic configuration of the oxygen molecule (O_2) which is shown in figure 2.8: The σ and the two bonding π -orbitals are fully occupied. Based on Hund's rule, the remaining two elec-

trons partly occupy the two antibinding π^* -orbitals with parallel spin. This gives rise to its paramagnetic and diradical character.

The two electrons with parallel spin form a spin-triplet, which is the ground state of molecular oxygen. There are five other possibilities to permute two electrons in two orbitals according to Fermi-Dirac statistics and Pauli's exclusion principle (Table 2.2): Triplet states 1 - 3 correspond to the three fold degenerate ground state ${}^3\Sigma_g^-$. The two-fold degenerate excited singlet state ${}^1\Delta_g$ (4 & 5) is approximately 0.98 eV higher in energy. A second singlet state, ${}^1\Sigma_g^+$, can be found ~ 1.63 eV above the ground state (6).³⁰

${}^1\Delta_g$ is, due to one unoccupied π^* -orbital, very electrophile and thus reactive. Additionally this state has a long radiative lifetime. For the unperturbed molecule the excited state lifetime was found to be $\tau_{\text{ex}} = 72$ min, whereas in polymers the radiative lifetime is least some tens of microseconds.³⁰

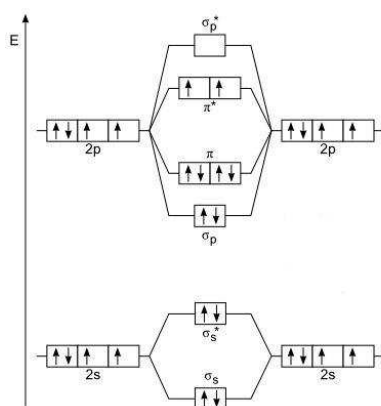


Figure 2.8: Molecular orbital diagram of the oxygen molecule (O_2) in its triplet ground state.

Table 2.2: Possible spin states in the two antibinding π MOs of the oxygen molecule.

#	π^*_x	π^*_y	#	π^*_x	π^*_y
1	\uparrow	\uparrow	4		$\downarrow\uparrow$
2	\downarrow	\downarrow	5	$\downarrow\uparrow$	
3	\downarrow	\uparrow	6	\uparrow	\downarrow

Oxygen is an important quencher of excited states of organic semiconductors. This is due to several reasons:³⁰

- The high oxygen concentration at ambient conditions.
- The small size of O₂ allows a very efficient diffusion into many organic materials.
- The two excited states of the oxygen molecule, ¹Δ_g and ¹Σ_g⁺ are usually lower in energy than the excited singlet state and triplet state of an OSC allowing efficient and irreversible energy transfer processes.

Possible quenching processes of excited triplet and singlet states are summarized in table 2.3.³⁰ However, they don't occur with the same probability. Typically the enhanced intersystem crossing pathways (S₁ → T_x) are dominant over S₁ → S₀ processes. The excess energy of the listed processes dissipates as heat. A detailed discussion on this topic and further literature can be found in [30, pp. 1721].

Eventually, the quenching process results in the formation of singlet oxygen. This process is commonly denoted as photosensitization. Singlet oxygen is a very reactive species and it is often responsible for the oxidation of hydrocarbons (e.g. the formation of carboxylic acids at alkyl chains or the addition to unsaturated carbon double bonds).^{41,59}

Table 2.3: Quenching processes of singlet and triplet states with ground state oxygen

Quenching of singlet states	Quenching of triplet states
$S_1 + O_2(^3\Sigma_g^-) \rightarrow T_1 + O_2(^1\Sigma_g^+)$	$T_1 + O_2(^3\Sigma_g^-) \rightarrow S_0 + O_2(^1\Delta_g)$
$S_1 + O_2(^3\Sigma_g^-) \rightarrow T_1 + O_2(^1\Delta_g)$	$T_1 + O_2(^3\Sigma_g^-) \rightarrow S_0 + O_2(^1\Sigma_g^+)$
$S_1 + O_2(^3\Sigma_g^-) \rightarrow T_1 + O_2(^3\Sigma_g^-)$	$T_1 + O_2(^3\Sigma_g^-) \rightarrow S_0 + O_2(^3\Sigma_g^-)$
$S_1 + O_2(^3\Sigma_g^-) \rightarrow T_2 + O_2(^3\Sigma_g^-)$	
$S_1 + O_2(^3\Sigma_g^-) \rightarrow S_0 + O_2(^3\Sigma_g^-)$	
$S_1 + O_2(^3\Sigma_g^-) \rightarrow S_0 + O_2(^1\Sigma_g^+)$	
$S_1 + O_2(^3\Sigma_g^-) \rightarrow S_0 + O_2(^1\Delta_g)$	

3 Polymer light emitting diodes

Besides photoexcitation, luminance can also result from an electronic current. This is for example realized in polymer light emitting diodes (PLEDs). Since the working principle of a PLED is already a well known topic nowadays, the basics will be kept short and the focus will be set on efficiency and device degradation.

3.1 Working principle

Electroluminescence can be observed after electronic excitation of an OSC. In principle one injects electrons into the LUMO and extracts them from the HOMO of the OSC by metal electrodes. A structural relaxation of the OSC as described in section 2.3 follows and polaron states are populated. If a positive and a negative polaron get attracted by Coulomb force, they can form an exciton - a bound electron-hole pair. The same pathways of deactivation of this excited state as in the case of photoexcitation are valid. (Section 2.4).

The injection of charge carriers is usually achieved with a device structure where an OSC is sandwiched between two conducting materials. During this process the charge carriers have to overcome a potential barrier, i.e. the energy difference between the work function of the electrode and the HOMO/LUMO level of the OSC. Thus the work function of the anode material should be as close as possible to the HOMO energy and the cathode work function should be as close as possible to the LUMO energy. The actual injection of the charge carriers is mainly described by the Fowler-Nordheim equation which describes field assisted tunneling of an electron through a potential barrier of certain shape. Also a thermionic injection, described by the Richardson-Dushman equation, is possible. However, its contribution at room temperature is rather low and field assisted tunneling is the dominant process.

The transport within the OSC can be regarded as a hopping movement of the charge carriers from one localized state to another. A measure of how quick a charge carrier can move in the OSC is given by the electron and hole mobility.

In order to achieve a balanced number of charge carriers within the light emitting layer, similar mobilities as well as similar anode/HOMO and LUMO/cathode potential barriers should be used.

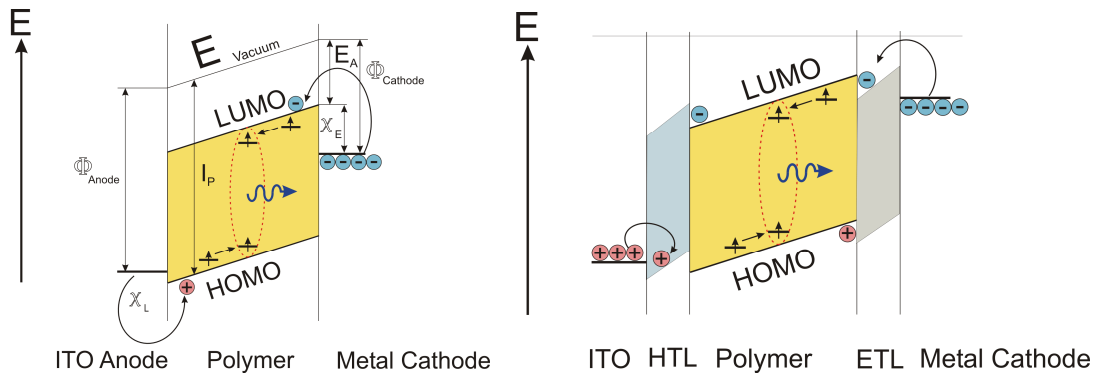


Figure 3.1: Energy level diagram of the basic OLED setup in single layer architecture (left) and as multi-layer setup (right). Taken from [31]

As one can see in figure 3.1 (left), the described conductor/OSC/conductor single layer structure is the most simple configuration. The more sophisticated multilayer approach facilitates an increased charge carrier injection by introducing a hole transport layer (HTL) between anode material and OSC and an electron transport layer (ETL) between OSC and cathode material, respectively. The HOMO level of the HTL is located between the HOMO of the active material and the work function of the anode material. The LUMO energy level of the HTL should be above the LUMO energy level of the active material to keep the electrons in the active layer. On the cathode side, the LUMO level of the electron transporter is located between the LUMO energy of the active material and the work function of the cathode. Hole blocking can be realized with a HOMO level higher in energy than the HOMO energy level of the emissive polymer.

The most common anode material is indium tin oxide (ITO) which is transparent for visible light. ITO is a large band gap semiconductor which gives rise to its transparency. Doping ensures the electrical conductivity. Usually poly(3,4-ethylenedioxythiophene) poly(styrenesulfonate) (PEDOT:PSS) is used as smoothing and hole injection layer between ITO and the active material. The chemical structure is shown in figure 3.2. PSS is an acid which possibly gives rise to later on discussed device degradation related processes.

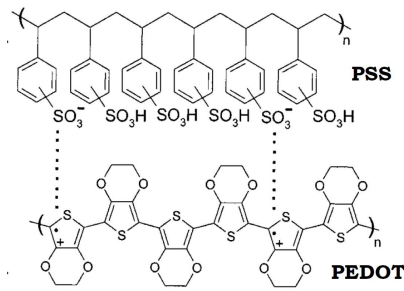


Figure 3.2: Chemical structure of PSS (upper polymer) and PEDOT (lower polymer)

Common cathode materials and material combinations are metals like silver or aluminium, alkaline earth metals like barium or calcium or also salts like caesium fluoride.

Location of the charge carrier recombination zone

Depending on the device setup (injection barriers at the electrodes, charge carrier mobilities and possible charge blocking layers), the charge carrier recombination zone can be assumed at different positions within the device. Figure 3.3 demonstrates this principle for cathode materials with different work functions. Cathode materials with a high work function and therefore bad electron injection efficiency can lead to a recombination zone near the cathode since the electrons are the minor species. A balanced charge carrier injection efficiency enables a recombination in the centre of the bulk. Low work function cathodes lead to a shift of the recombination zone towards the anode since the major injection barrier is located at the anode.

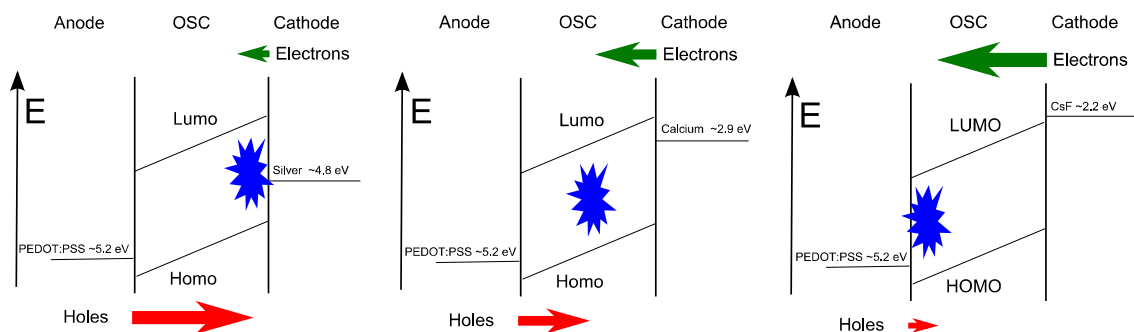


Figure 3.3: Schematic picture of the shift of the exciton recombination zone by the application of different cathode materials. Left: Hole-majority; Middle: Balanced charge carrier injection; Right: Electron-majority.

3.2 Electroluminescence quantum yield

A general definition of the quantum efficiency (η) of a PLED is the ratio of the number of photons which leave the device over the number charge carriers injected. η made up of different terms,

$$\eta = \Phi_{PL} \cdot r_{st} \cdot \gamma \cdot X . \quad (3.1)$$

η ... Electroluminescence quantum efficiency; Φ_{PL} ... PLQY; r_{st} ... Fraction of excitons which are able to recombine radiatively; γ ... Fraction of excitons formed; X ... Other decreasing factors;

γ is the number of excitons formed over the number of charge carriers injected. The number of dissociative excitons is also taken into account. γ can be improved by ensuring balanced charge carrier injection and by introducing charge blocking materials between electrodes and active layer.

r_{st} stands for the number of excitons which are able to recombine radiatively over the total number of excitons created, i.e. the singlet-triplet ratio in fluorescent materials. Basic spin statistics predict that in PLEDs 25% of the created excitons are singlets, while 75% are triplets. There is a lot of discussion ongoing about the validity of this approach. Different studies claim that the singlet fraction could exceed the predicted 25%.³² The latest publications showed, however, again that the expected 1/4-singlet, 3/4-triplet ratio is justified.³³ This limit can be overcome by the use of phosphorescent materials, where also triplet excitons are able to recombine radiatively. Internal quantum efficiencies close to 100% are thus possible in theory.

Φ_{PL} is the number of singlet excitons that recombine radiatively. An excited state can release its energy on different pathways without emitting a photon (section 2.4), and this, of course, lowers the overall efficiency. Φ_{PL} is equivalent to the corresponding value obtained by photoluminescence spectroscopy, where it's defined as the number of photons emitted over the number of photons absorbed. Thus, Φ_{PL} can be measured using photoluminescence spectroscopy. Since all terms in equation (3.1) are smaller or equal than unity, a study of Φ_{PL} provides information about the ultimate maximum electroluminescence quantum efficiency that can be achieved.

The last term in equation (3.1) comprises several light-output reducing factors such as self-absorption in the active layer or light interference and total reflection at the interfaces. Also all types of quenching are included by this factor.

Measurement of the electroluminescence quantum yield

Although the actual measurement of the electroluminescence quantum yield is not topic of this work, a short description of the recommended experimental method is given here for the sake of completeness: The most accurate method would be to place the device in an integrating sphere (Figure 3.4), which then collects the emitted photons independent of the emission angle. However, one has to keep in mind that not every created photon will be detected since there certainly occurs self-absorption within the active layer or re-absorption by transport layers. Also, the detector signal has to be converted into terms of number of quanta. An example how to achieve this for photomultiplier tubes is given in section 4.6. A detailed instruction to measure the electroluminescence quantum yield can be found in [34].

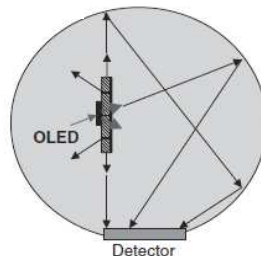


Figure 3.4: Integrating sphere with a mounted devices to measure the electroluminescence quantum yield. Taken from [34].

3.3 Device degradation and related processes

The long time spectral stability and luminance stability of PLED devices are basic demands for commercialization of this technology. Especially for blue emitting polymers the desired spectral stability was not achieved so far. Some of the known degradation mechanisms are described below. It was already stated, that different parameters influence the charge carrier recombination zone within the device: An electron minority can lead to a recombination near the cathode; balanced hole-electron ratios might lead to a

centered recombination and an electron majority shifts the recombination zone towards the anode. Hence, in the sections 3.3.2 - 3.3.4 the spectral stability of the emission originating from the corresponding device region is discussed. However, the first topic here deals with the spectrally stable decrease of the electroluminescence emission intensity.

3.3.1 EL quantum yield reducing factors

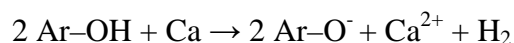
The reduction of the electroluminescence quantum yield of a PLED during time is an often observed but poorly understood process. However, at least for phosphorescent materials a luminescence reducing process was explained by oxygen quenching.⁶⁶ Due to the long excited state lifetime of triplet excitons ($\sim\mu\text{s}$), this emission can efficiently be quenched by diffused oxygen. The fact that the emission intensity partly recovers after reducing the amount of oxygen in the active layer strongly indicates that the dominant process is dynamic quenching. A reduction of the emission intensity can be observed for fluorescent materials as well. In this case the observed reduction of the emission intensity may not be explained with quenching by oxygen entirely: The excited state lifetime of a singlet state is many orders of magnitude lower ($\sim\text{ns}$) than of triplets which makes a diffusive encounter with oxygen within this time more unlikely. Furthermore, it can be stated that in PLEDs the number of triplet excitons exceeds the number of singlet excitons by far (only every fourth created exciton is a singlet; singlets have a much lower lifetime than triplets). Thus it seems to be much more probable that oxygen quenches a triplet exciton.

However, also for fluorescent materials the emission intensity partly restores upon the reduction of oxygen. Similar effects can be observed for humidified atmospheres.

3.3.2 Organic / Cathode interface

In order to improve the electron injection from the cathode and thus the overall device efficiency, low work function materials like barium (work function $\phi_{\text{C}} = 2.6 \text{ eV}$), calcium ($\phi_{\text{C}} = 2.9 \text{ eV}$) or caesium fluoride ($\phi_{\text{C}} = 2.2 \text{ eV}$) are used. A major drawback of these materials is their high reactivity to oxygen and humidity as well as the toxicity of some of their byproducts (e.g. oxides or hydroxides). The usually used barrier layer of aluminum cannot exclude interactions with H_2O and O_2 completely.⁶

For example, poly(fluorene) based devices with calcium or aluminum electrode often show two unwanted red-shifted emission peaks around 480 nm and 520 nm.³⁵ A possible explanation was given by Kappaun et al.³⁶, who proposed a deprotonation reaction of hydroxy end chain units by diffused calcium:



Another cathode related degradation mechanism is the formation of non-emissive device regions which are commonly denoted as dark spots. Mainly they are caused by delamination of the electrode material due to moisture and the applied operation voltage: H₂O can reach regions under the cathode via pin-holes caused by contaminations during the fabrication. Subsequent, the driving voltage of the device induces the electrochemical dissociation of water according to $2 \text{ H}_2\text{O} + 2\text{e}^- + \text{ H}_2 + 2\text{OH}^-$. The hydrogen gas creates bubbles and delaminates the cathode.³⁷

3.3.3 Anode / Organic interface

In nearly every efficient PLED device, PEDOT:PSS is used as a smoothing and hole-transport layer. Further more, it reduces the injection barrier for holes. After spin-coating, a thin PSS-rich layer is formed on the top of the film^{38,39}. It was shown by different studies^{61,67,68}, that PSS can cause trap states within the emissive polymer. Most likely this is due to an acidic interaction of PSS with the active polymer. Especially for nitrogen containing polymers it's known that the lone electron pair of nitrogen is easy to protonate, which subsequently leads to spectral shifts.⁵⁷ Also electrophilic addition reactions with unsaturated electron-rich carbon double bonds (e.g. in PPV) are proposed.^{61,62}

3.3.4 Bulk material

Besides the influences of cathode or anode materials, also chemical modifications of single monomer units in the polymer bulk can lead to optical instabilities. In poly(fluorene) based emitter polymers, for example, an oxidative degradation mechanism can lead to the formation of fluorenone units⁴⁰ (keto-defects). These defects act as charge carrier traps and usually lead to a broad emission in the green spectral region already at low ketonic-defect concentrations. Their formation can either happen already during synthesis - which is related to an incomplete alkylation at the 9-position of the

fluorene unit, or during device operation. Among others, the latter can be assigned to the creation of singlet oxygen (see section 2.5.2), which then attacks the alkyl side-chains of the polymer. Via different intermediates (cleaved side chains and side chains with carboxylic acid units), this process ends in the formation of ketonic defects.⁴¹

4 Experimental methodology

The scope of this chapter is a description of the applied spectroscopic methods as well as the corresponding sample preparation to obtain the photophysical characteristics of organic semiconductors. Moreover, an indirect method to measure the photoluminescence quantum yield for solutions will be presented. This chapter closes with the preparation and characterization process for PLEDs.

4.1 Solution and thin film preparation

All samples were processed and stored under argon atmosphere.

Solutions were prepared using toluene (spectrophotometric grade; Sigma-Aldrich) as solvent. For the actual UV/VIS and PL measurements, quartz cuvettes from HELMA Analytics with a light path of 10 mm were used.

Thin films were prepared by spin-coating from solution on glass substrates. Substrates were cleaned thoroughly with deionized water, acetone and 2-propanol and in an ultrasonic bath. The spin-coating process was done with a DELTA6 RC spin coater (SÜSS MicroTec Lithography GmbH) under argon atmosphere using the rotation parameters 1000 rpm/12 s for the actual film formation followed by 3000 rpm/40 s for drying. The concentrations of the solutions depend on the individual experiment and will be mentioned in the corresponding chapters.

4.2 Layer thickness measurements

All layer thicknesses were measured with a VECCO Nanoman VS atomic force microscope.

4.3 Optical absorbance measurements

The absorbance of a material at a certain wavelength is given by Beer-Lamberts law,

$$A = \log_{10}\left(\frac{I_0}{I}\right). \quad (4.1)$$

A ... Absorbance; I_0 ... Intensity of the incident light; I ... Intensity of the transmitted light;

The measurements were performed on a PERKIN ELMER LAMBDA 900 UV/VIS – spectrometer. I_0 was obtained by measuring the transmitted light either of the blank glass substrate in case of thin films or of the solvent filled quartz cuvette for solutions. The instrument permanently monitors and corrects the incident light beam and hence no further correction was necessary.

In order to get significant absorbance signals, solutions in the concentration range 0.01 g/l - 1 g/l and films up to 40 nm thickness were chosen.

4.4 Photoluminescence measurements

As already described in section 2.4, the radiative recombination of an excited state created by light is called photoluminescence. Two spectrofluorophotometer of the type SHIMADZU RF-5301PC were used to measure these spectra.

To exclude any self-absorption or inner filter effects⁴³, dilution series of the polymer solution in the range from 10^{-9} g/l to 10^{-3} g/l were prepared and photoluminescence was measured. Films were spin-coated from 1 g/l solution (if not stated otherwise) in order to keep them thin.

Figure 4.1 shows the working principle of the SHIMADZU RF-5301PC spectrometer.

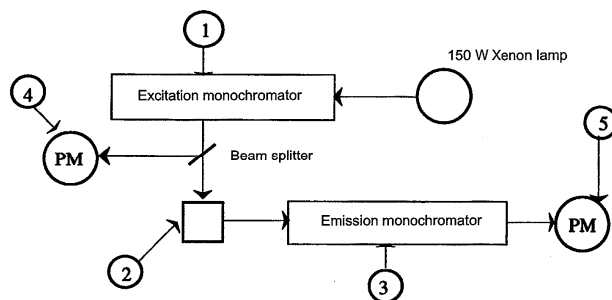


Figure 4.1: Principle setup of the SHIMADZU RF-5301PC spectrofluorophotometer. 1: Excitation monochromator; 2: Cell / sample holder; 3: Emission monochromator; 4:PMT to monitor the excitation light; 5: Detector PMT. Taken from [42]

An 150 W xenon lamp is used as excitation light source. A certain wavelength for the excitation of the sample can be chosen by a first monochromator. The emitted light is tuned by an emission monochromator and detected by a photomultiplier tube (PMT). Each of these optical components distorts the obtained spectrum which makes a careful calibration necessary. The biggest effect stems from the photocathode of the PMT since its response strongly depends on the used material (e.g. different alkali alloys).

4.5 Calibration of a spectrofluorophotometer

Different spectrometers can lead to the detection of significantly different emission spectra of one and the same sample which makes the interpretation and comparison of the measured spectra difficult. Especially for measurements of the photoluminescence quantum yield, exact emission spectra are of big importance. Consequently, a calibration process is presented in the following.

Light source calibration

The light source, which in case of the SHIMADZU RF-5301PC is a 150 W Xenon lamp, does not have a uniform intensity output over the spectral region of interest. Therefore samples excited by a wavelength of higher intensity, lead to a higher photoluminescence signal, even if the absorbance of the material is lower than at other energies. Generally one has to do this correction 'by hand'. However, the used instrument is equipped with a light source compensation system which permanently monitors a frac-

tion of excitation light by an additional PMT (see figure 4.1 - #4) and then electronically corrects the obtained spectra. Thus this correction can be omitted.⁴²

Detection system calibration

The basic idea behind a calibration of the detection system is to compare a well known emission spectrum of a reference material with the measured spectrum of the same material. By this method, the instruments spectral responsivity can be obtained by following formula⁴³,

$$S(\lambda) = \frac{I(\lambda)}{L(\lambda)}. \quad (4.2)$$

S ... Total responsivity of the instrument; I ... Known emission of the reference material; L ... Measured emission.

The Federal Institute of Materials and Testing (BAM) recently developed five dyes which exhibit certified emission spectra in the range from 300 nm to 770 nm for exactly this purpose.^{44,45} The actual calibration process is given by following standard operation procedure⁴⁶:

1. Preparation of the calibration solutions under argon atmosphere. Solvent: ethanol.
2. Choice of the excitation wavelength, dependent of the dye.
3. Measurement of background spectra with pure solvent as sample to correct any scattering artifacts from the cuvette or the solvent.
4. Measurement of the actual solution repeatedly (> 10 times) and averaging.
5. Repeat step 2 – 4 for all 5 dyes

Figure 4.3 shows the normalized collected and certified emission spectra of the five dyes.

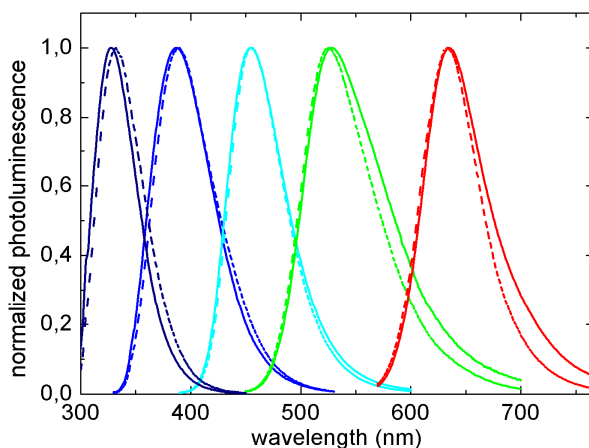


Figure 4.2: Normalized emission spectra of the BAM certified dyes; from BAM-F001 (high energy spectrum) to BAM-F005 (low energy spectrum). Solid lines: measured spectra; Dotted lines: certified spectra.

As mentioned, the responsivity curve can now be calculated by dividing the five certified spectra through the five measured spectra. Merging these five individual correction curves leads to the global responsivity curve for the spectrometer in the range between 300 nm and 770 nm. This evaluation was done by the software LINKCORWIN 1.1.0.0 (provided by BAM). A detailed description of the process can be found elsewhere.^{46,47}

The described calibration was done for two instruments of the same type (SHIMADZU RF-5301PC). Figure 4.3 presents the calculated responsivities.

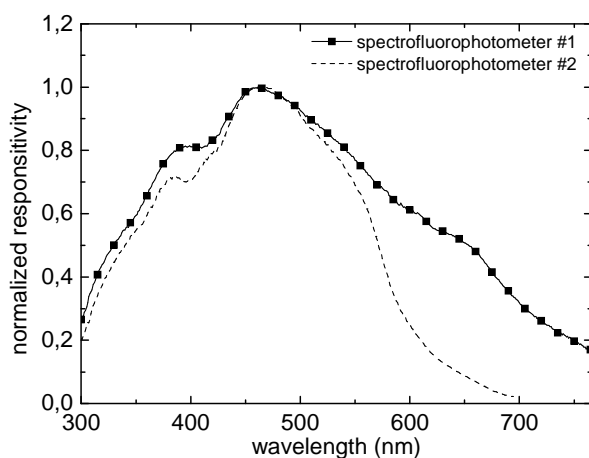


Figure 4.3: Calculated responsivities of two SHIMADZU RF-5301PC spectrometers.

Although both instruments should have the same PMT⁴², one can easily see the sharp cut-off of the responsivity in the infrared region for one of the instruments (dashed line) and other differences in the shape. This fact demonstrates that one can not be sure that two spectrometers of the same type have the same responsivity and a calibration should be performed for each instrument.

4.6 Photoluminescence quantum yield (for solutions)

As mentioned, the PLQY is a basic photophysical property defined by

$$\Phi = \frac{\text{number of photons emitted}}{\text{number of photons absorbed}}. \quad (4.3)$$

A direct measurement of the latter values would require special optical equipment which was not available during this work. Therefore an indirect method, using standard laboratory equipment and a reference material with known PLQY, was employed. This method was already proposed in the 1960s and is widely accepted nowadays.^{48,49} However, an error < 10% should be assumed.^{50,51} The basic idea behind this method is to compare absorbance and total emission of a reference material with the corresponding values of the sample by using following equation,

$$\Phi_x = \Phi_r \cdot \left(\frac{n_x}{n_r}\right)^2 \cdot \left(\frac{A(\lambda_r)}{A(\lambda_x)}\right) \cdot \left(\frac{I(\lambda_r)}{I(\lambda_x)}\right) \cdot \left(\frac{D_x}{D_r}\right). \quad (4.4)$$

Subscript x ... Sample; Subscript r ... Reference; Φ ... PLQY; n ... Refractive index; A ... Absorbance; I ... Excitation light intensity; D ... Value proportional to the total number of photons emitted.

The fraction which accounts for different excitation light intensities, $I(\lambda_r)/I(\lambda_x)$, can be omitted, since the used instruments is equipped with a light source compensation system (see section 4.5)

As reference material, quinine sulphate dihydrate (obtained from Sigma Aldrich; chemical structure and absorbance spectrum and photoluminescence spectrum are shown figure 4.4) with a PLQY of $\Phi_r = 54\%$ ⁴³ was chosen.

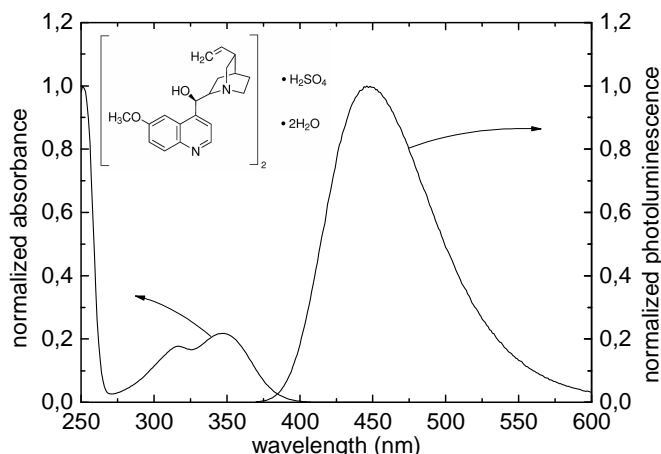


Figure 4.4: Chemical structure of Quinine sulphate dihydrate and the corresponding absorbance spectrum and photoluminescence spectrum.

Quinine sulphate is not quenched by oxygen, i.e. its PLQY is the same under inert atmosphere and in air.⁵² Therefore solutions were prepared under ambient conditions using 0.5M-sulphuric acid as solvent.

The refractive index correction accounts for the fact that the emitted light gets refracted at the solution/cuvette/air interfaces in different magnitudes dependent on the index of refraction of the sample solution and different fractions of light can reach the detector.⁴⁹ This principle is sketched in figure 4.5.

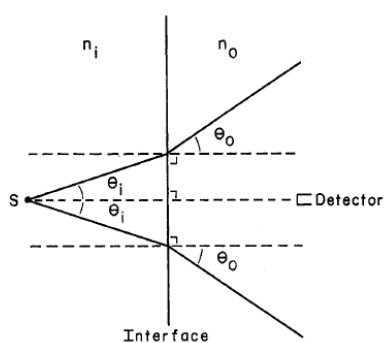


Figure 4.5: Refraction occurs on the solution/cuvette/air interface in different angles θ , dependent on n_i , the refractive index of the solution. Taken from [49].

The absorbance fraction relates to different absorbance values at the wavelength of interest (i.e. the excitation wavelength for photoluminescence measurement).

The last term in equation (4.4) accounts for the different amounts of emitted light in terms of a value directly proportional the total number of emitted photons. Since the PMT of the spectrometer gives a signal proportional to the energy of the incoming photons and not to the number of photons, further conversions are needed. Table 4.1 explains the way from the detector output signal towards a value direct proportional to the number of emitted photons.

Table 4.1: Conversion from PMT output to a value directly proportional to the number of photons emitted

	Name	Unit
1.	Detector output, M	$\left[\frac{A}{nm} \right]$
2.	Responsitivity, S	$\left[\frac{A}{W} \right]$
3.	Corrected spectrum, $R = \frac{M}{S}$	$\left[\frac{A}{nm} \right] / \left[\frac{A}{W} \right] = \left[\frac{W}{nm} \right] \sim \left[\frac{eV}{s \cdot nm} \right]$
4.	Conversion to number of quanta per s·nm, $Q = R \cdot \lambda$	$\left[\frac{quanta}{s \cdot nm} \right]$
5.	Total number of quanta, $\int Q \cdot d\lambda$	$\left[\frac{quanta}{s} \right]$

Since integrated emission over absorbance simply is the gradient of this linear relationship, one can minimize concentration dependent effects and measurement errors by replacing equation (4.4) by

$$\Phi_x = \Phi_r \cdot \left(\frac{Grad_x}{Grad_r} \right) \cdot \left(\frac{n_x}{n_r} \right)^2. \quad (4.5)$$

Subscript x ... Sample; Subscript r ... Reference; Φ ... PLQY; Grad ... Gradient of absorbance vs. integrated emission relationship; n ... Refractive index

The gradients are calculated by measuring absorbance and integrated emission of many different concentrations. Integrated emission over absorbance should give a linear relationship; a linear regression gives the gradient. Points of high absorbance which obviously deviate from the linear slope indicate self absorption or inner filter effects and should be omitted. The example for quinine sulphate is given in figure 4.6: The squares indicate the measured absorbance and integrated emission for different concentrations,

the red solid line is a linear fit through these points. Two points of high absorbance deviate from the expected linear relation and were not considered in the linear regression.

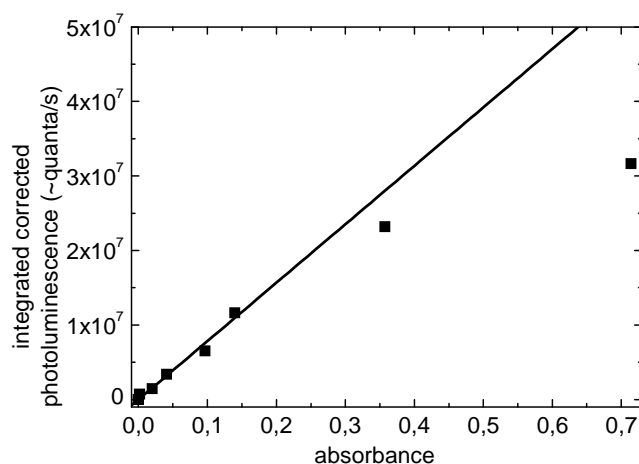


Figure 4.6: Absorbance over integrated photoluminescence emission in terms of quanta per second. black squares: measured points; red line: linear fit through zero. The points of high absorbance which obviously deviate from the linear relation were not considered in the fit.

Quantum yield measurement for thin films

The presented approach for the PLQY evaluation for solutions is not fully applicable for solids such as thin films. Different additional effects like light polarization and angular dependence of the emitted light have to be taken into account. Also, the quantum yield may heavily depend on the film thickness (self-absorption) and film morphology and thus a suitable standard cannot be realized. The most accurate way to measure this value would be with an integrating sphere in order to count the photons independent of the emission angle. At least relative statements are possible when the reference material and the sample are similar. The quantum yield of the investigated polymers in this work were compared to dioctylfluorene, a common poly(fluorene) derivate. Absorbance- and emission spectrum as well as the chemical structure of dioctylfluorene are depicted in figure 4.7.

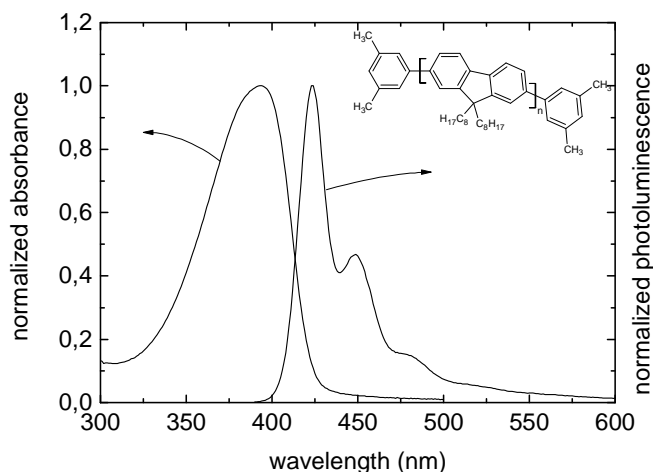


Figure 4.7: Absorbance spectrum, emission spectrum and chemical structure of dioctylfluorene.

4.7 PLED device preparation

The device preparation and characterization was carried out in a ISO-Class 6 clean room facility at the NTC Weiz Forschungsgesellschaft mbH.

ITO coated glass substrates with a sheet resistance of 15 ohm/sq were structured by etching with 37%-diluted HCl. Several subsequent cleaning steps with deionized water, acetone and 2-propanol in an ultrasonic bath for 15 minutes followed. For better adhesion of the deposited PEDOT:PSS layer (Clevios P VP AI 4083 from H.C. Starck), the cleaned ITO substrate was plasma activated for 15 minutes in an oxygen plasma at a base pressure of 0.3 mbar. PEDOT:PSS was spin-coated with 2500 rpm for 40 s which led to an average layer thickness of ~60 nm. To remove any residual solvent, the layer was annealed at 120°C in high vacuum ($< 5 \cdot 10^{-3}$ mbar) for one hour and afterwards cooled down to room temperature. The electrooptical active layer as well as the optional hole transport layer were also brought up by spin-coating from toluene solution. Layer thicknesses and annealing parameters were changed during the individual experiments and will be described in the corresponding chapters. The optional electron transport layer (TPBi) and the cathode, comprising aluminum or a calcium/aluminum double layer were thermally evaporated in an fully automated evaporation chamber at a base pressure $< 10^{-6}$ mbar. Evaporation rates and resulting thicknesses will be stated in the corresponding chapters. The final device was mounted and characterized in a sealed measurement chamber.

The basic characterization includes,

- Voltage-current characteristics, recorded with a KEITHLEY 2612 sourcemeter (computer assisted),
- Simultaneous measurement of the emitted light intensity using a silicon-diode and a KEITHLEY 6417A electrometer,
- Photocurrent – luminance calibration with a MINOLTA LS-100 luminance meter,
- Measurement of the electroluminescence emission spectrum using a LOT-ORIEL CCD-spectrometer

5 Photophysical characterization of poly(indenofluorene)-based polymers

The photophysical properties of three novel poly(indenofluorene)-based emitter polymers and one novel poly(indenofluorene)-based hole transporting material were investigated in this chapter. UV/VIS-spectroscopy and photoluminescence spectroscopy on solutions and thin films were made and their photoluminescence quantum yield was evaluated. Moreover, the fabrication of multi-layer structures with the hole transporting polymer and the emitter polymers, which is a basic requirement for the application in PLEDs, was examined.

5.1 Emitter materials

All materials were found to be perfectly soluble in chloroform and toluene. The latter was used as solvent for all solutions.

Poly(indenofluorene) homopolymer

This material is a typical poly(indenofluorene) homopolymer (denoted as *homoPIF* in the following) with side chains on every bridgehead. It was used as reference material for the later on presented copolymerized species and its photophysical properties are shown in figure 5.1. The thin film emission spectrum shows significant intensity from ~400 nm to ~550 nm with a maximum at 424 nm and a vibronic fine structure at around 449 nm. The unstructured absorption spectrum has its maximum at around 405 nm resulting in a Stokes-shift of 19 nm. In contrast to the film emission, the emission maximum of the solution is 8 nm blue-shifted due to solvatochromism and appears at 416 nm with a vibronic fine structure at 441 nm. Maximum absorbance was found at 402 nm (Stokes shift: 14 nm) and the photoluminescence quantum yield in solution is $\Phi=94\%$.

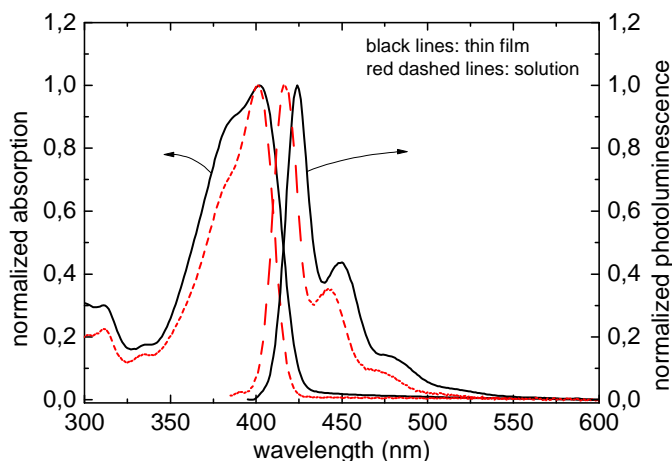


Figure 5.1: Normalized absorbance spectra and photoluminescence spectra of *homoPIF* in solution (dashed red line) and in thin film (solid black line)

Since the evaluation of the PLQY is straightforward following equation (4.5), a more detailed description is given only for this material. The integrated emission versus absorbance gradient of the quinine sulphate reference was already shown in section 4.6. Basically, one has to measure these two parameters for different concentrations of *homoPIF*: A dilution series in the range from 10^{-8} g/l to 10^{-1} g/l was prepared. However, concentrations lower than 10^{-4} g/l were not useable because of the obtained signals were dominated by noise. Dilutions higher than 10^{-2} g/l led to significant self absorption. As depicted in figure 5.2, the remaining concentrations gave a good linear relationship.

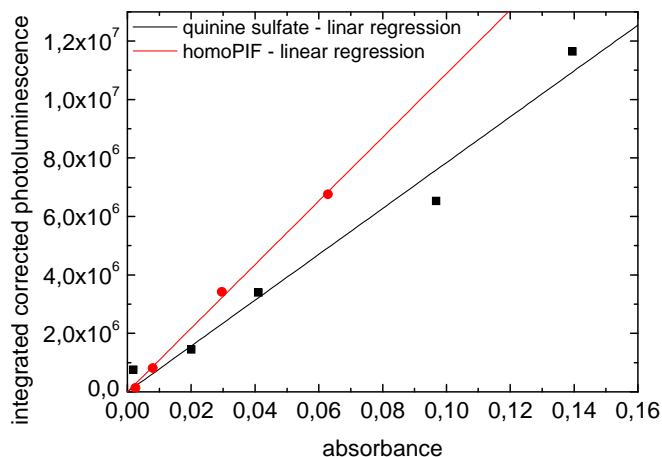


Figure 5.2: Measured points and linear fit of quinine sulphate (measurement: black squares, fit: black line) and of *homoPIF* (measurement: red circles, fit: red line)

The slope of the *homoPIF* fit is steeper than in the case of quinine sulfate and therefore its PLQY is higher than that of the reference material. The necessary refractive indices of toluene ($n=1.4969$) and sulfuric acid diluted in deionized water ($n=1,345$) are taken from literature.⁵³ Now equation (4.5) can be applied, leading to a PLQY of $\Phi=94\%$. A PLQY of 102% (relative to dioctylfluorene) was found for thin films.

Poly(indenofluorene) copolymer 1

The backbone of this copolymer (denoted as *coPIF-1*) consists of the previously studied *homoPIF* and of small amounts of a triphenylamine-based unit.

Absorbance- and the photoluminescence spectra of *coPIF-1* can be found in figure 5.3 (left).

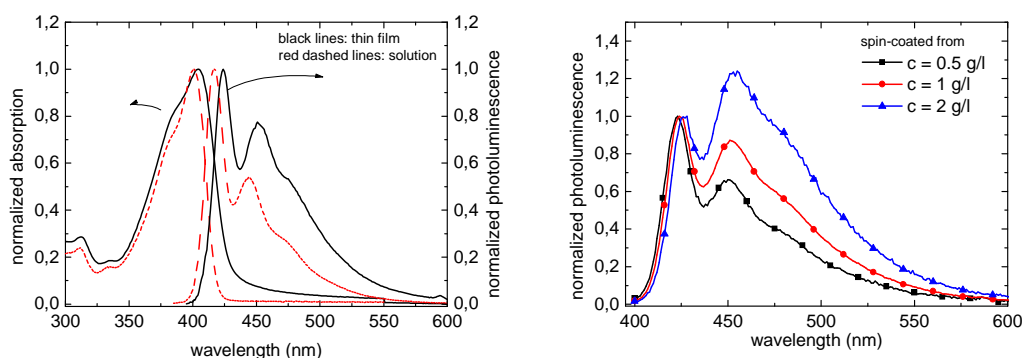


Figure 5.3: Left: Normalized absorbance spectra and photoluminescence spectra of *coPIF-1* in solution (dashed red lines) and in thin film (solid black line); Right: Dependence of the film emission spectrum on the concentration of the parent solution (and thus of the resulting layer thickness)

The thin film spectrum reveals significant emission from ~ 400 nm to ~ 600 nm with a maximum at 424 nm and compared to *homoPIF* a stronger vibrational maximum around 451 nm. The unstructured absorption spectrum has its maximum around 404 nm resulting in a Stokes-shift of 20 nm. In contrast to the film emission, the emission maximum of the solution is slightly blue-shifted due to solvatochromism and appears at 417 nm with a vibronic fine structure at 444 nm. The maximum absorbance can be found at 401 nm. Its Stokes-shift is thus around 16 nm. Strong film thickness dependencies of the emission spectrum were found (Figure 5.3, right). The photoluminescence quantum

yield in solution is $\Phi = 87\%$. The thin film PLQY measurement led to $\Phi = 95\%$ (relative to dioctylfluorene).

Poly(indenofluorene) copolymer 2

The backbone of this second copolymer (denoted as *coPIF-2*) consists of the previously studied *coPIF-1* and of small amounts of a phenylene-vinylene based unit.

Absorbance- and photoluminescence spectra of *coPIF-2* are depicted in figure 5.4 (left).

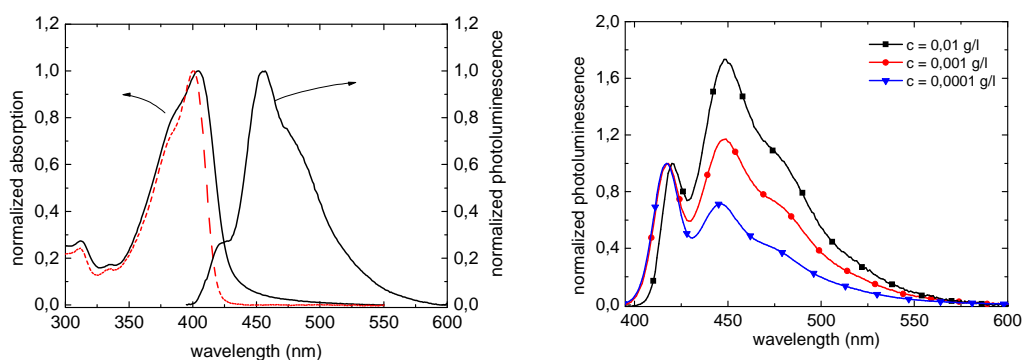


Figure 5.4: Left: Normalized absorbance spectra and photoluminescence spectra of *coPIF-2* in solution (dashed lines/red) and in thin film (solid black line). Right: Concentration dependence of *coPIF-2* solutions to the emission spectrum

The photoluminescence emission of a thin film expands from 400 nm to 550 nm and shows a maximum at 457 nm with shoulders around 422 nm and 475 nm. According to its chemical structure and the weak emission at 422 nm, an efficient energy transfer from poly(indenofluorene) to the emitting phenylene-vinylene units can be assumed. The unstructured absorption spectrum has its maximum around 404 nm resulting in a Stokes-shift of 53 nm. Maximum absorbance for the solution was found at 401 nm. The photoluminescence signal of *coPIF-2* solutions is significantly dependent on the used polymer concentration (Figure 5.7, right). The emission maximum at 457 nm decreases with increasing solid content. This is apparently due to the decreasing intermolecular contact between single polymer chains for higher dilutions resulting in a suppressed interchain energy transfer to the phenylene-vinylene units. A photoluminescence quantum yield of $\Phi = 77\%$ was found in solution. Thin film measurements led to $\Phi = 93\%$ (relative to dioctylfluorene).

5.2 Hole transport material

Generally hole transport materials have a low ionization potential and a low electron affinity.⁵⁴ The HOMO level should be localized between that of the commonly used PEDOT:PSS (HOMO energy: 5.2 eV) and the HOMO of the emitter polymer. In order to realize electron blocking, a LUMO energy lower than that of the emitter is favorable (see section 3.1).

The solution processable hole transport material *htlPIF* is a copolymer with equal amounts of poly(indenofluorene) and triphenylamine based units in its backbone. The fact that the *htlPIF* is also perfectly soluble in toluene leads to fabrication related problems in multilayer structures. The following sections deal with this topic.

5.2.1 Photophysical properties of *htlPIF*

Absorbance- and the photoluminescence spectrum of *htlPIF* can be found in figure 5.5

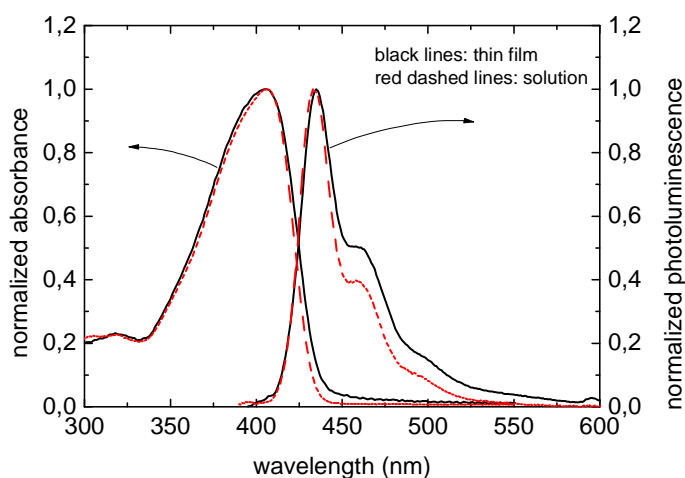


Figure 5.5: Normalized absorbance and photoluminescence of *htlPIF* in solution (red dashed lines) and as thin film (black solid line).

The thin film emission shows a maximum at 435 nm with a less pronounced vibronic fine structure maximum at 461 nm. The unstructured absorption spectrum has its maximum at 406 nm resulting in a Stokes-shift of 29 nm. The PL-emission of the *htlPIF* solution has its maximum at 435 nm with a shoulder at 461 nm and an absorbance maximum at 406 nm (Stokes-shift: 29 nm). No significant differences between thin film

and solution spectra were found. The photoluminescence quantum yield in solution is $\Phi = 87\%$ and in thin film $\Phi = 124\%$ (relative to dioctylfluorene).

5.2.2 Fabrication of multi-layer structures

As mentioned, fabricating multi-layer structures from solution can be challenging. It has to be ensured that the solvent of the subsequently deposited material does not dissolve any subjacent layer. This can be realized by different approaches, including the use of materials with orthogonal solubility⁵⁵ or cross-linking polymers. Orthogonal solubility means that the first involved polymer is only soluble in its distinct solvent and insoluble in the solvent of the second involved polymer. This is not given in case of *htlPIF* and the emitter PIFs since both are perfectly soluble in toluene. So it has to be elucidated if *htlPIF* shows any thermally activated cross linking properties⁵⁶. Therefore, thin films were spin-coated on PEDOT:PSS and annealed in HV at 70°C for 1 h. Subsequently, the polymer layer was treated with the pure solvent under spin process conditions. Before and after the spin coating of toluene, the layer thickness was measured by AFM. Independent of the layer thickness (up to 100 nm), a complete dissolving was found. Thus, the process is not suitable for multi-layer fabrication. In order to increase the film stability, the annealing temperature was increased to 200°C. No detectable reduction of the coated layer thickness was found after toluene treatment. However, such high temperatures are capable to change the emission properties of the polymers due to the formation of chemical defects. To exclude any changes in absorbance and photoluminescence spectra, these parameters were measured before and after annealing. No changes were found (Figure 5.6, left). Note that annealing in air led to the development of a broad pronounced emission centered around 590 nm (Figure 5.6, right).

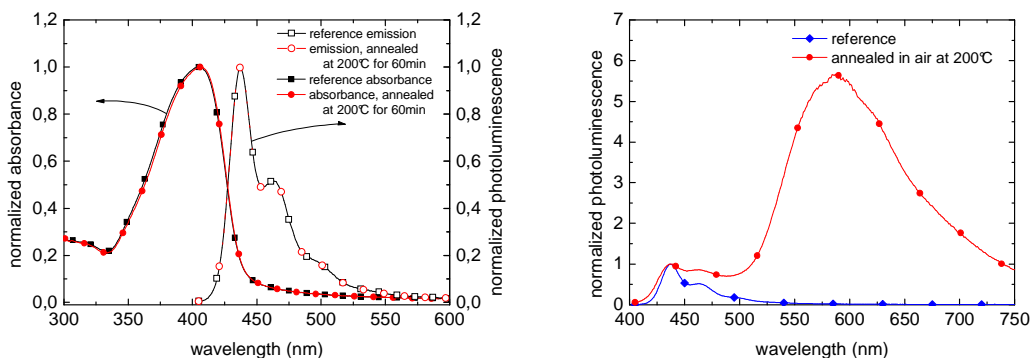


Figure 5.6: Left: Absorbance (full symbols) and emission (open symbols) of htlPIF before (black squares) and after (red circles) annealing at 200°C in argon atmosphere. Right: Emission after 1 h at 200°C in ambient conditions.

5.3 Summary and discussion

Figure 5.7 comprises the thin film emission spectra of *homoPIF*, *coPIF-1* and *coPIF-2*. The impacts of the slightly different chemical structures can be seen easily. *homoPIF*, which is a pristine PIF, shows the expected emission spectrum. A strong enhancement of the second maximum can be found in the case of *coPIF-1* with its amine based units. The emission spectrum of *coPIF-2* suggests a very efficient energy transfer from the PIF unit to the phenylene-vinylene units. Photoluminescence measurements of *coPIF-2* solutions with low concentrations revealed a suppression of this energy transfer. This is apparently due to decreasing intermolecular contact between single polymer chains. The photoluminescence quantum yield is high for all three polymers, making them good candidates for applications as active layers in PLED.

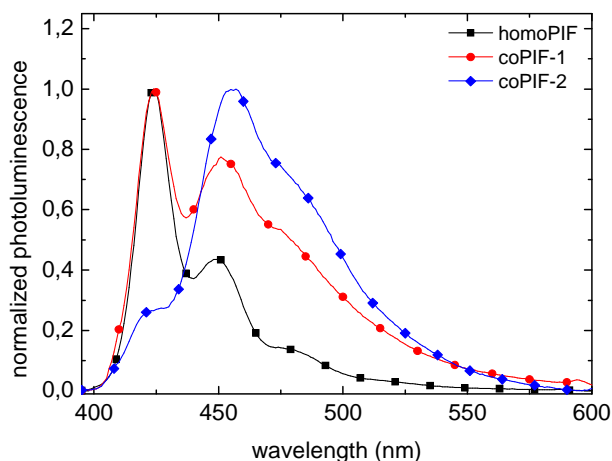


Figure 5.7: Normalized thin film emission spectra of *homoPIF* (black/squares), *coPIF-1* (red/circles) and *coPIF-2* (blue/diamonds).

The hole transport material *htlPIF* shows blue emission and a high photoluminescence quantum yield as well. Its emission maximum is red-shifted with respect to *homoPIF* and *coPIF-1*. Since the band gap is smaller than that of those two polymers, there won't be any energy barrier for electrons between them. Besides that, its good solubility in toluene is a problem for multi-layer PLED applications. No dissolving of the thin film was not found for 200°C bake-out temperature and the photoluminescence spectrum was stable. Nevertheless, a partial dissolvment of the layer after subsequent polymer deposition cannot fully be excluded.

6 Photoluminescence related material stability

A prerequisite for the application of light emitting polymers in PLEDs is their spectral stability to ambient and chemical influences. Several approaches to investigate these influences are presented in this chapter.

6.1 Stability with respect to thermal stress

Thin polymer films were spin-coated on glass substrate and annealed under ambient conditions and under argon atmosphere. The photoluminescence spectrum was measured immediately after spin-coating and after 30 min, 1 h, 2 h, 3 h, 4 h and 5 h incremental annealing. During annealing, ambient light was excluded in order to avoid any UV-induced effects.

6.1.1 homoPIF

The degradation series of *homoPIF* under ambient conditions is shown in figure 6.1 in a qualitative way (normalized to the second maximum, left) and in a quantitative way (right). The latter were normalized to the maximum emission intensity of the untreated sample, which allows a comparison of the absolute intensities. Degradation under argon can be found in figure 6.2.

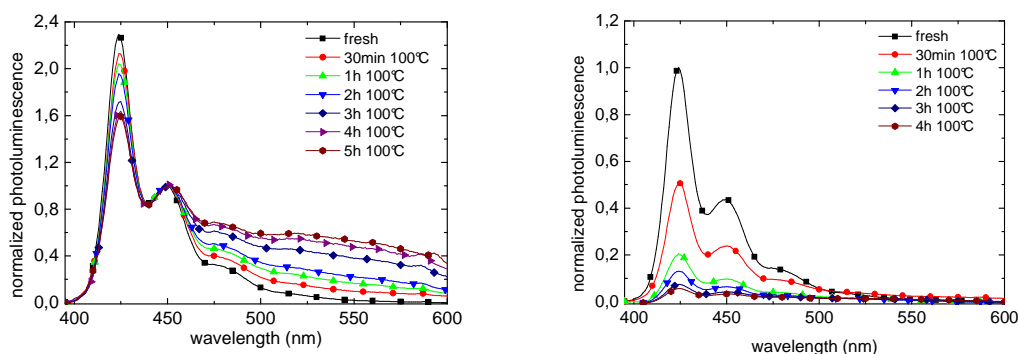


Figure 6.1: Thermal degradation series at 100°C of *homoPIF* under ambient conditions. Left: Normalized to the second maximum; Right: Normalized to the emission maximum of the untreated sample.

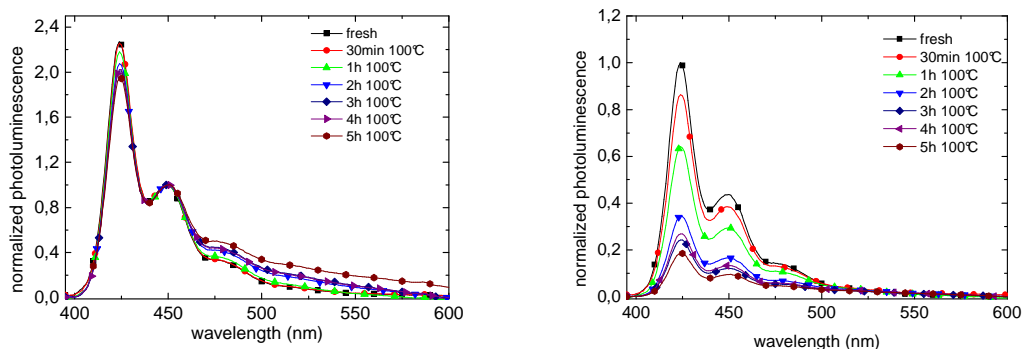


Figure 6.2: Thermal degradation series at 100°C of *homoPIF* under argon. Left: Normalized to the second maximum; Right: Normalized to the emission maximum of the untreated sample.

In both cases the overall emitted intensity decreased significantly. After 5 hours at 100°C the absolute intensity at 424 nm decreased in the case of argon atmosphere by a factor of ~ 4 and in case of ambient conditions by a factor of ~ 20 . Normalized spectra of the thin film treated under argon reveal a decrease of the maximum emission at 424 nm and a slight enhancement of the emission in the spectral region between 480 nm and 600 nm (Figure 6.2, right). Similar, but much more pronounced changes were found for films annealed under ambient conditions.

Due to the higher loss of intensity and the lower stability under ambient conditions, the investigated effects can clearly be assigned to interactions with oxygen and/or humidity.

Reversibility studies

Besides chemical changes of the emissive unit due to a singlet-oxygen reaction, also dynamic or static quenching processes are conceivable to cause the overall reduction of the emitted photoluminescence intensity. At least for dynamic quenching from oxygen or humidity it should be possible to restore parts of the original emitted intensity by reducing previously diffused oxygen or water from the film. Therefore two thin films were prepared and annealed for 2 h under ambient conditions. Afterwards one film was kept in high vacuum ($< 10^{-5}$ mbar) at room temperature for 2 hours, the other film was kept in high vacuum at 100°C for 2 hours. PL spectra were measured after each step. The sense of annealing the second sample under HV was to introduce some additional energy into the system in order to break up possible ground-state complexes which

would cause static quenching. figure 6.10 shows the development of the intensity over time. It can clearly be seen that the emitted intensity did not recover. Hence, at least dynamic quenching can be excluded.

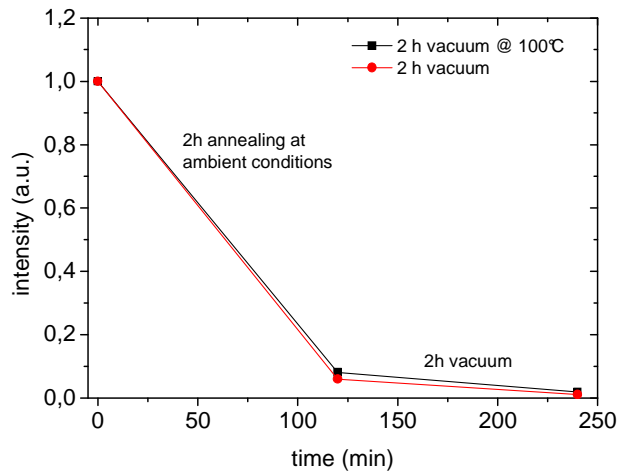


Figure 6.3: Photoluminescence intensity over time for two spin coated homoPIF films. A 2 h annealing is followed by a 2 h HV step (red line/circles). Additional annealing in HV at 100°C (black line/squares).

6.1.2 coPIF-1

The thermal degradation series under ambient conditions for *coPIF-1* can be found in figure 6.4. Related to the 0-1 transition, a slight decrease of the emission maximum can be found. The emission between 500 nm and 600 nm heavily increases. After 5 h at 100°C the absolute emitted intensity decreased by a factor of ~ 10 . Similar, but less pronounced effects were found after annealing under argon atmosphere (see figure 6.5). The absolute intensity decreased by a factor of ~ 4 .

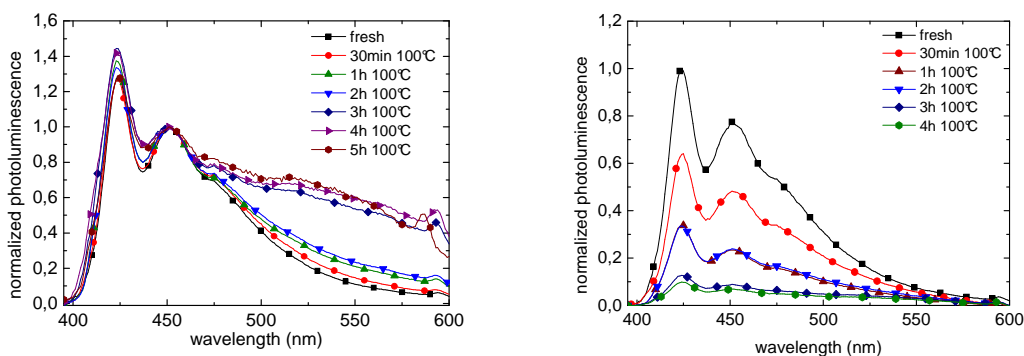


Figure 6.4: Thermal degradation series at 100°C of coPIF-1 under ambient conditions. Left: Normalized to the second maximum; Right: Normalized to the emission maximum of the untreated sample

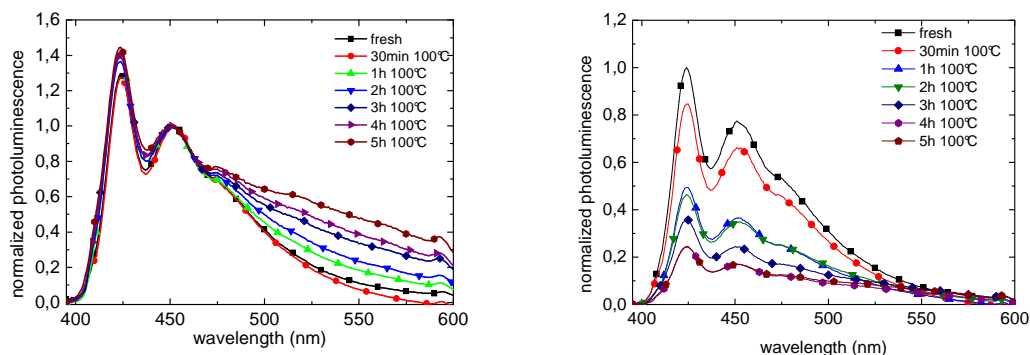


Figure 6.5: Thermal degradation series at 100°C of *coPIF-1* under argon. Left: Normalized to the second maximum; Right: Normalized to the emission maximum of the untreated sample.

Again, this behavior clearly indicates an oxygen and/or humidity induced effect. Compared to *homoPIF*, *coPIF-1* shows a reduced spectral stability which thus can be assigned to the amine side-chains.

6.1.3 *coPIF-2*

Strong spectral instabilities were found for *coPIF-2*. The degradation series under ambient conditions (Figure 6.6) reveals a strong relative decrease of the phenylene-vinylene emission with a maximum around 457 nm. The PIF emission becomes more significant. Already after 1 h annealing, the *coPIF-2* emission is similar to that of *coPIF-1*, which indicates the complete deactivation of the phenylene-vinylene emission. Also the emission between 500 nm and 600 nm increased. This may be related to the formation of ketonic defect states. The same effects can be observed for annealing in argon. However, parts of the original emission still remain after 4 h annealing. After 4 hours at 100°C the maximum intensity at 457 nm decreases in the case of argon atmosphere by a factor of 6 and in the case of ambient conditions by a factor of 20. A detailed discussion about this behavior can be found in section 6.4.

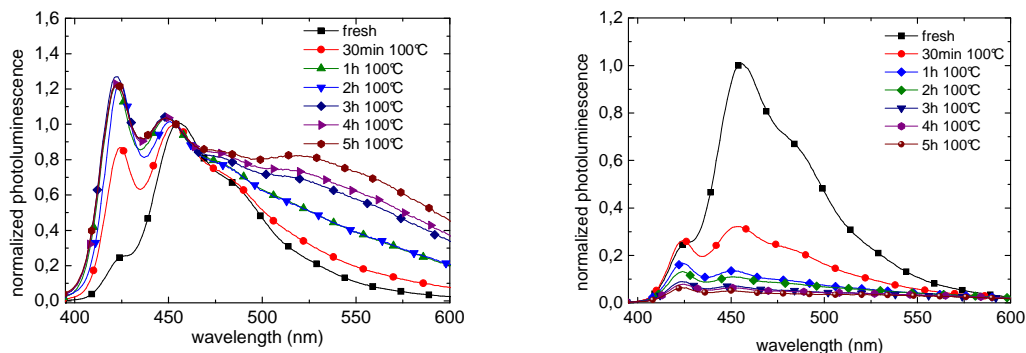


Figure 6.6: Thermal degradation series at 100°C of coPIF-2 under ambient conditions. Left: Normalized to the original emission maximum around 457 nm; Right: Normalized to the emission maximum of the untreated sample.

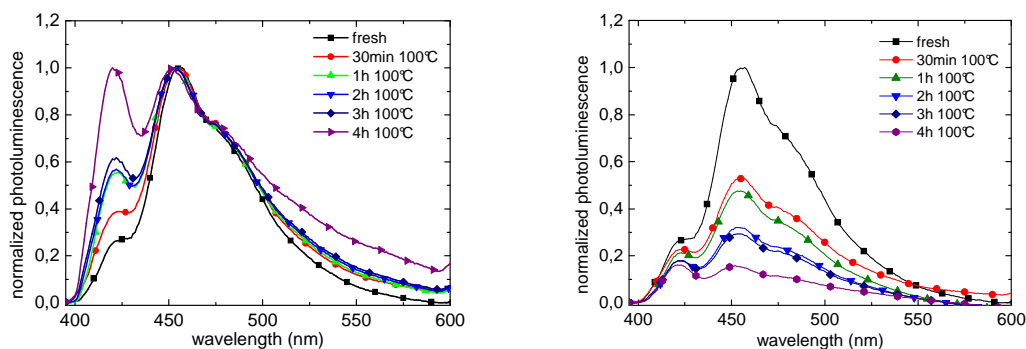


Figure 6.7: Thermal degradation series at 100°C of coPIF-2 under argon. Left: Normalized to the original emission maximum around 457 nm; Right: Normalized to the emission maximum of the untreated sample.

6.2 Stability with respect to UV irradiation

Previous photoluminescence measurements pointed out that two measurements, one immediately after the other, already show different emission intensities. Therefore, the excitation process itself can be made responsible for this effect. This process is commonly known as photobleaching and is caused by different reasons dependent of the chemical structure of the fluorophore. Mostly it's an oxygen-induced effect.

For the investigation of the stability of *homoPIF*, *coPIF-1* and *coPIF-2* with respect to these effects, thin films of the polymers were spin coated and mounted in the measurement chamber of a SHIMADZU RF-5301PC spectrofluorophotometer. A definite exci-

tation wavelength was chosen via the excitation monochromator. To ensure large area irradiation, the excitation slits were set to their maximum aperture. This led to an irradiated area of $\sim 5 \text{ mm} * 5 \text{ mm}$. The irradiation was interrupted by PL measurements after certain time intervals (up to six minutes). The results of this experiment are depicted in figure 6.8. The left column presents the degradation series for an irradiation wavelength of $\lambda_{\text{IRR}} = 280 \text{ nm}$, the right column the series for $\lambda_{\text{IRR}} = 380 \text{ nm}$.

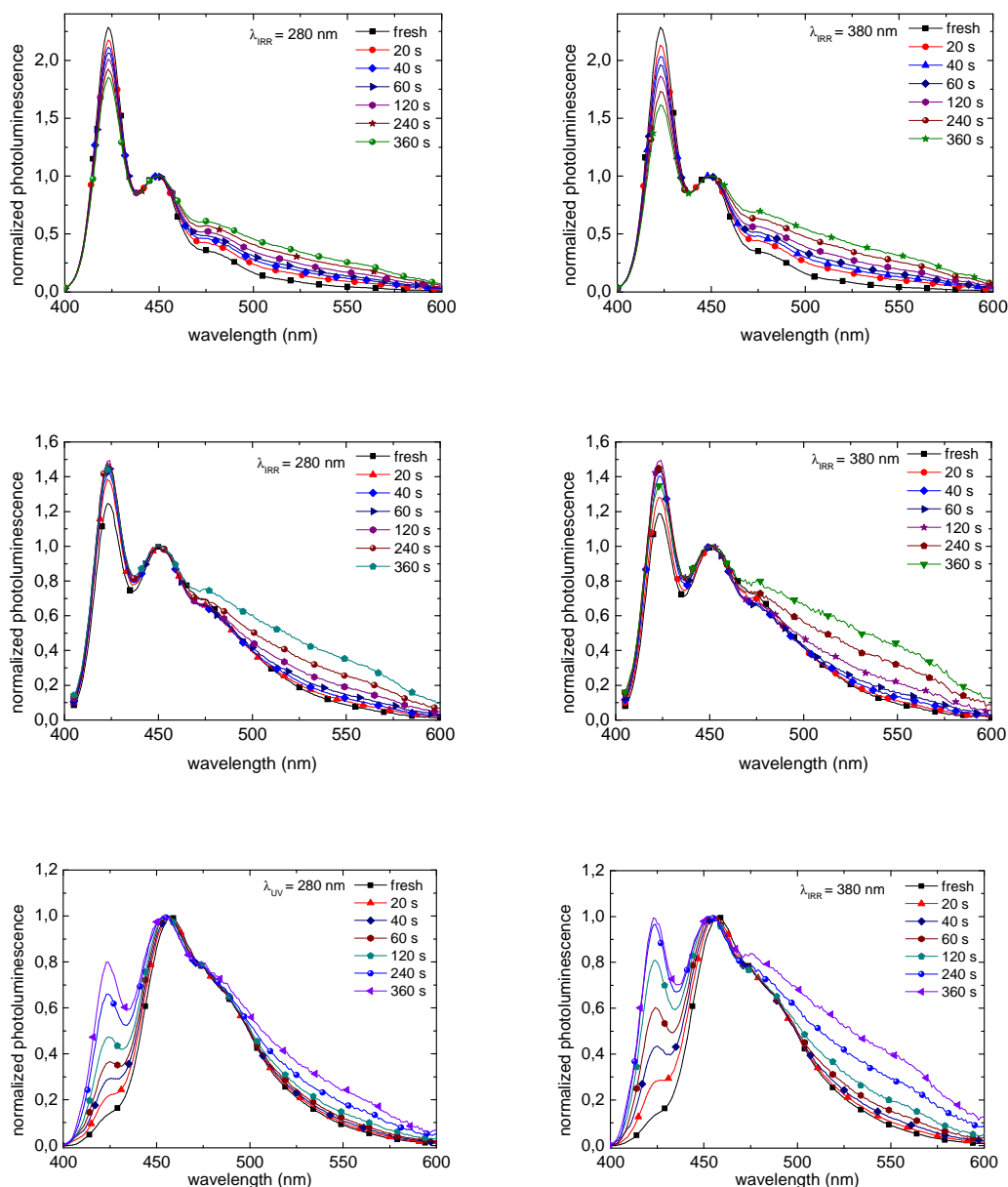


Figure 6.8: Continuous excitation of the polymers *homoPIF* (top), *coPIF-1* (middle) and *coPIF-2* (bottom) with UV light. Excitation with $\lambda_{\text{IRR}} = 280 \text{ nm}$ (left) and $\lambda_{\text{IRR}} = 380 \text{ nm}$ (right).

The UV irradiation results are similar to that obtained during thermal treatment, but on a lower timescale: *homoPIF* and *coPIF-1* show good stability with minor decreases of the emission maximum at 424 nm. Also, an increase of the emission between 500 nm and 600 nm was found. The maximum intensity decreased for *homoPIF* by a factor of ~ 6 at $\lambda_{\text{IRR}} = 380$ nm and by a factor of ~ 5 in the case of $\lambda_{\text{IRR}} = 280$ nm, respectively. *coPIF-1* emission intensity decreased in both cases by a factor of ~ 4 . The most significant changes of the PL emission showed *coPIF-2*. Relative to the emission maximum, the shoulder at around 424 nm increased strongly during treatment. The intensity of the emission maximum, however, decreased by a factor of ~ 15 in both cases. For all three polymers, the spectral changes were stronger for the irradiation with $\lambda_{\text{IRR}} = 380$ nm. At a first glance, this seems to be contradictory because the high energy radiation with 280 nm caused less damage. This becomes clearer when we look at the absorption spectra of the three polymers (Chapter 5). The maximum is located near 380 nm and only a low absorption can be found around 280 nm. This leads to the suggestion that the degradation process is excitation related. A discussion on this is given in section 6.4.

The next section deals with measurements on sealed samples in order to elucidate the influence of oxygen and humidity.

Sealed samples

The previously described experiment was repeated using a sealed sample of *homoPIF*. Basically the polymer solution was spin coated on a glass substrate, covered with a second glass substrate and sealed with epoxy. Note that it was only possible to irradiate the sample with $\lambda_{\text{IRR}} = 380$ nm due to the high absorption of the glass sealing in regions lower than 350 nm. The result of the investigation is presented in figure 6.9.

Nearly no spectral changes were observed and the maximum intensity decreased only by a factor of ~ 2 . So the enhanced overall stability can be ascribed to the exclusion of oxygen and humidity realized by the sealing.

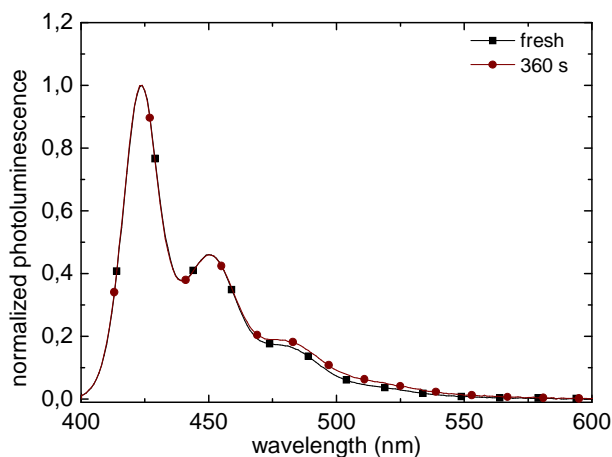


Figure 6.9: Continuous excitation of a sealed homoPIF film. $\lambda_{\text{IRR}} = 380$ nm.

This result of a reduced stability for the excitation wavelength where the polymer has higher absorption as well as the increased stability for sealed films leads to the assumption that not the UV irradiation itself damages the polymer, but the highly reactive singlet oxygen (section 2.5.2), created during a photosensitization process does.

6.3 Stability with respect to acidic environments

Motivated by the work of Kappaun et al.⁵⁷, who demonstrated protonation and deprotonation reactions of the active layer which consequently led to spectral instabilities, acidic influences on *homoPIF*, *coPIF-1*, *coPIF-2* and *htlPIF* were investigated. Due to its popularity and its acidic character, any PEDOT:PSS induced effects are of special interest. Furthermore, the influences of a strong organic acid - trifluoroacetic, and an inorganic acid - hydrochloric acid were analyzed.

6.3.1 PIF / PEDOT:PSS double layers

In nearly every efficient PLED PEDOT:PSS is used as a smoothing and hole transporting layer between ITO and the active material. It was supposed, that due to its acidic character, its film-forming properties and its possible diffusion into the active material (see theory section 3.3.3 for details), an interaction with the active material at the interface is possible.

To investigate possible effects with photoluminescence spectroscopy, PEDOT:PSS (~60 nm)/PIF double layers were fabricated. The possible effect was expected to be limited to the interfacial region, hence the deposited PIF layer had to be very thin (spin-coated from 0.1 g/l solution). Reference samples (polymer solely on glass substrates) from the same solutions were fabricated as well. Figure 6.10 shows the results for *homoPIF*, *coPIF-1*, *coPIF-2* and *htlPIF*.

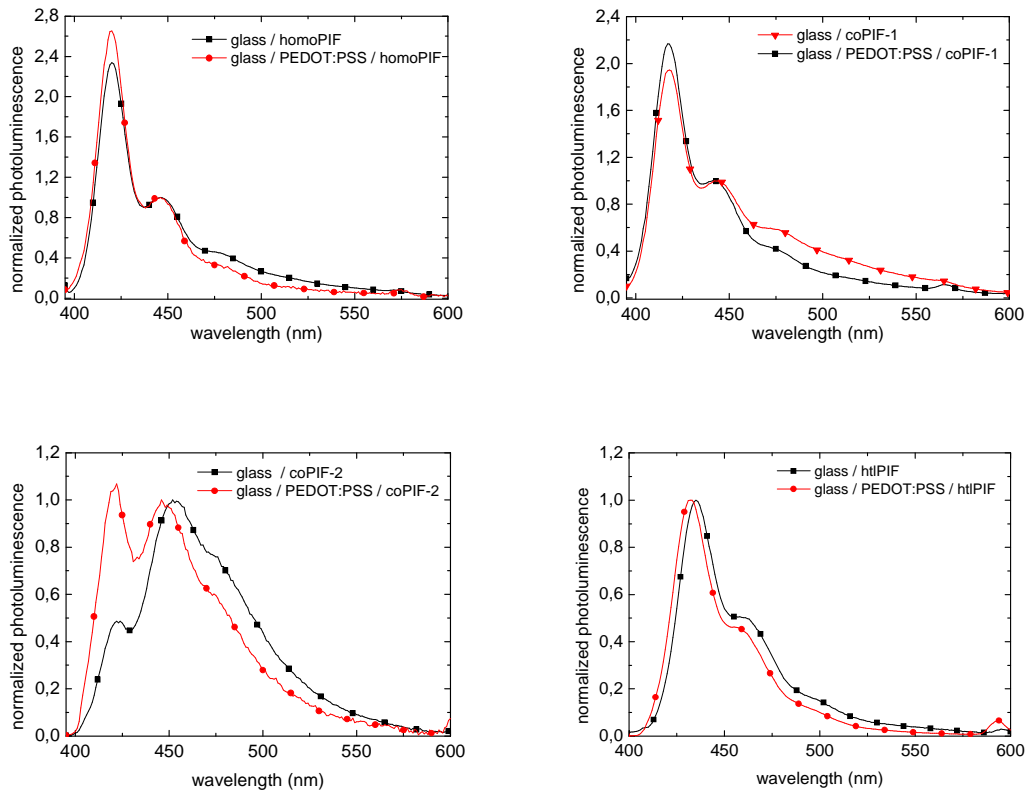


Figure 6.10: PL spectra of PEDOT:PSS/polymer double layers (black line/squares) and reference spectra of the polymer solely (red line/circles). top left: *homoPIF*; top right: *coPIF-1*; bottom left: *coPIF-2*; bottom right: *htlPIF*.

homoPIF and *coPIF-1* showed good stabilities - no significant changes due to the subsequent PEDOT:PSS layer were found. However, significant changes were observed in the case of PEDOT:PSS/*coPIF-2* double layers. Compared to the single layer systems they showed a significantly enhanced peak around 424 nm. Beside a blue shift of 3 nm, the PEDOT:PSS/*htlPIF* double layer system showed no significant changes of the optical properties of *htlPIF* due to an interaction with the PEDOT:PSS layer

6.3.2 PIF / Trifluoroacetic blends

For further clarification of any acid-induced effect, trifluoroacetic (TFA) in different concentrations was added to the parent solutions and subsequent spin-coated on glass substrate. TFA ($\text{CF}_3\text{-COOH}$) is a strong organic acid and is, compared to other acids, perfectly soluble in organic solvents like toluene, which of course was the basic requirement for this experiment. PL spectra of the results can be found in figure 6.11.

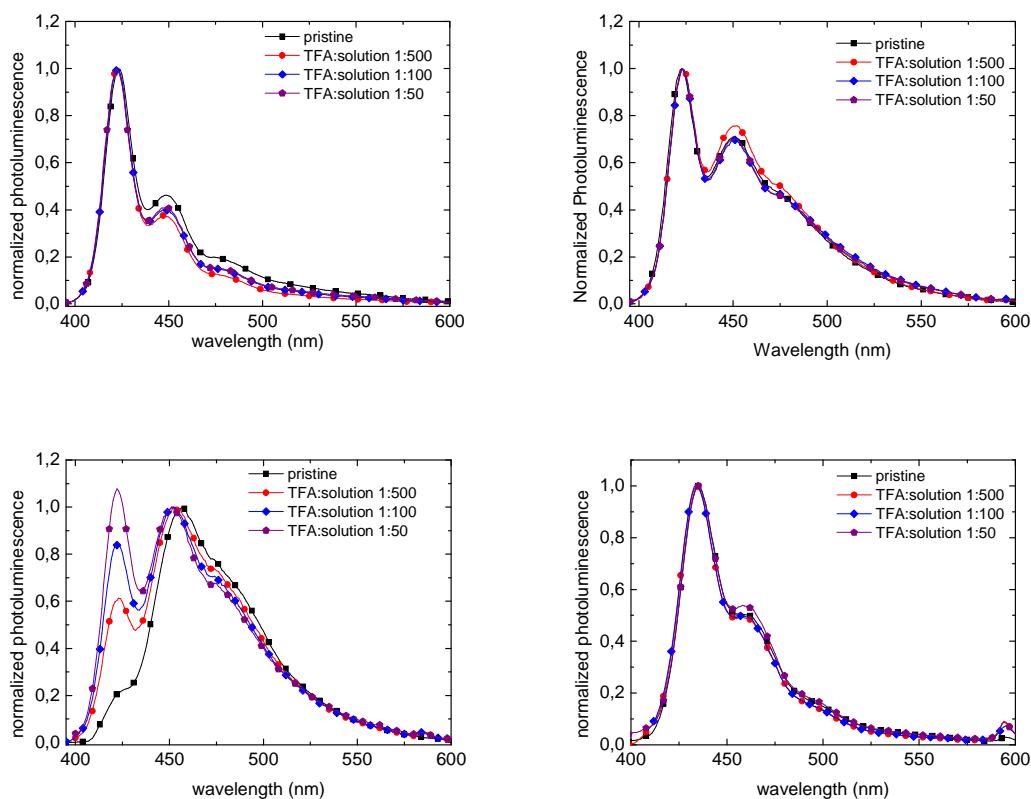


Figure 6.11: PL spectra (normalized to the emission maximum) of polymer solution/TFA blends with different ratios (see legend). top left: *homoPIF*; top right: *coPIF-1*; bottom left: *coPIF-2*; bottom right: *htPIF*.

Again, a no significant spectral changes for *homoPIF*, *coPIF-1* and *htPIF* were measured. Especially the good spectral stability of *coPIF-1* and *htPIF* was not expected since they have amine-based transport groups: The nitrogen atom of the latter, with its lone electron pair in the valence shell, acts as base and can easily be protonated, which can lead to spectral changes.^{57,58}

The emission characteristics of *coPIF-2* showed changes, similar to all previous degradation studies: The PIF emission around 424 nm becomes more significant compared to the phenylene-vinylene emission with increasing acid concentration.

6.3.3 PIF / HCl interactions

To investigate interactions with an inorganic acid, the samples were held over an open bottle of fuming HCl for ~3 s. The photoluminescence spectra of the subsequent measurement can be found in figure 6.12.

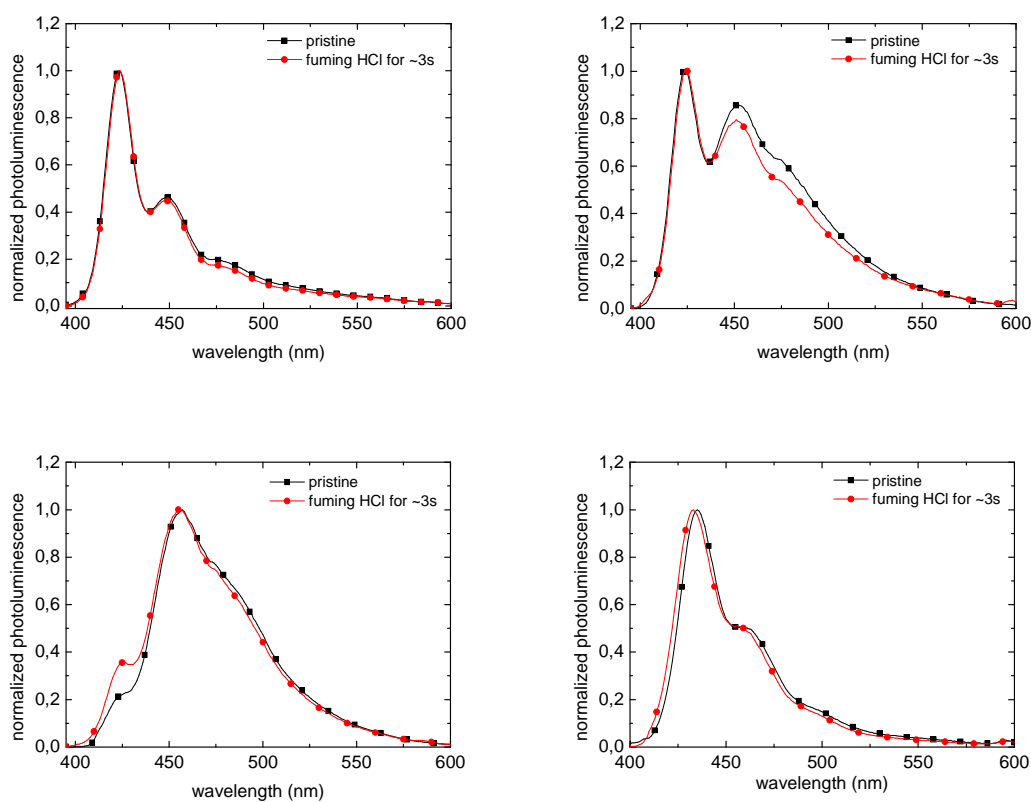


Figure 6.12: PL spectra (normalized to the emission maximum) of polymer films exposed to HCl fume (red line / circles) and reference measurements of the unexposed sample (black line / square). top left: homPIF; top right: *coPIF-1*; bottom left: *coPIF-2*; bottom right: htlPIF.

The investigated effects were very limited which can be due to the short interaction time. However, they correspond with the results obtained with polymer solution/trifluoroacetic acid blends.

6.4 Summary and discussion

A good spectral stability can be assigned to *homoPIF* and *coPIF-1*: Changes during all kinds of treatment were limited, but always related to a relative decrease of the emission maximum at 424 nm and an increase of the relative emission between 480 nm and 600 nm. The biggest effect was found for thermal treatment under ambient conditions, which suggests oxygen and/or humidity induced effects. Absolute emission intensities always strongly decreased. The fact that no restoring of the emission intensity was found after a 2 hour lasting HV storage, leads to the exclusion of dynamic quenching as causing factor.

Irradiation with UV-light ($\lambda_{\text{IRR}} = 380$ nm and $\lambda_{\text{IRR}} = 280$ nm) also led to the described effects, whereas the samples showed a decreased stability for low energy irradiation. The absorbance of the polymers is higher for irradiation with $\lambda_{\text{IRR}} = 380$ nm so it can be suggested that this is a excitation related effect. Sealed samples showed increased stability. This leads to the presumption that singlet oxygen (created by a photosensitized process, see chapter 2.5.2) might react with the polymer, introducing chemical defects and thus non-emissive units or spectral shifts. No significant acid-induced effect was found for *homoPIF* and *coPIF-1*.

The poly(indenofluorene) copolymer with amine and phenylene-vinylene based units, *coPIF-2*, showed a similar remarkable behavior during all kinds of treatment. Related to the emission maximum at 457 nm, the shoulder at 424 nm developed to a pronounced peak. This can be assigned to the deactivation of the phenylene-vinylene emission. A possible process occurring during UV irradiation would be related to the formation of singlet oxygen. Singlet oxygen can add in a [2+2] cycloaddition to the doubly bonded carbon atoms of the vinylene unit leading to a dioxetane intermediate. Then it's proposed that this adduct breaks down into two aldehydes.^{59,60} This principle is shown in figure 6.13

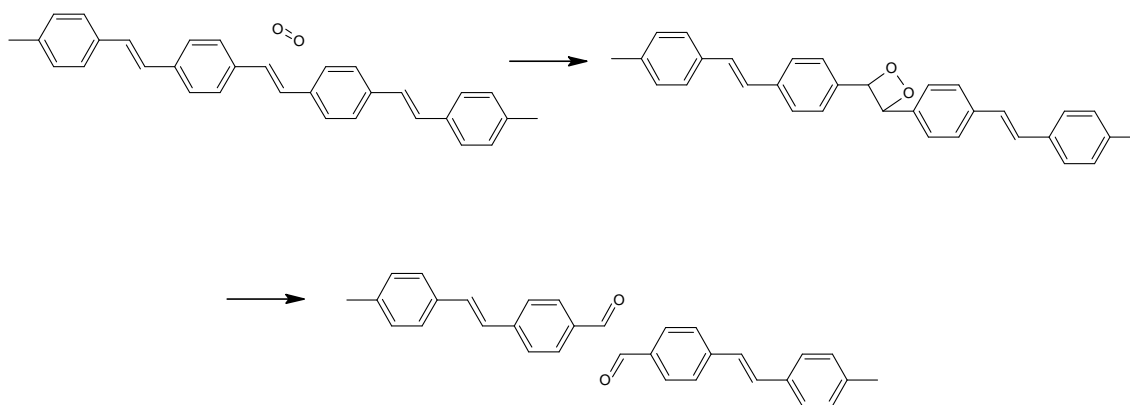


Figure 6.13: Proposed chemical reaction between phenylene-vinylenes and singlet oxygen responsible for the deactivation of the phenylene-vinylene emission.

This, however, does not explain the alike results for the PEDOT:PSS/coPIF-2 heterostructures, the blends with trifluoroacetic acid and the treatment with fuming HCl. Obviously, these effects are caused by the acidic environment. A possible reaction may be given by an electrophilic addition of the acid to the unsaturated carbon double bond.^{61,62} This bond consists of a strong σ -bond and a weaker π -bond. The latter acts as nucleophile, attracting the electrophile part of molecules. This would be the hydrogen atom in case of acids. The H^+ -proton adds to one of the doubly bonded carbon atoms, leaving the second carbon atom positively charged and singly bonded. The latter forms a bond with the remaining negatively charged acid radical, creating a non-emissive unit. Find the proposed reaction for HCl in figure 6.14: The more positive part of the polarized bond between hydrogen and chloride gets attracted of the electron rich vinylene bond and forms a bond with one carbon atom. The remaining Cl^- acid radical reacts with the second, now positively charged carbon atom.⁶³ This principle can be applied for TFA and PSS as well.

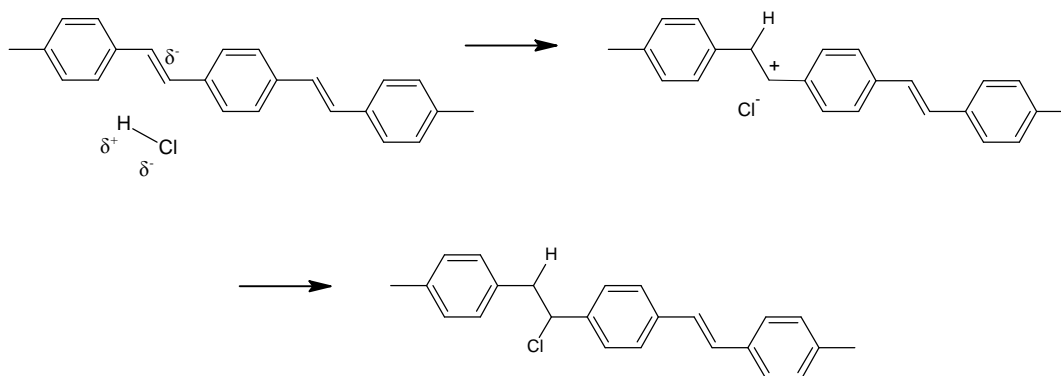


Figure 6.14: Electrophilic addition of HCl to the double bond of the phenylene-vinylene unit.

Minor effects were observed for *htlPIF*. The PEDOT:PSS/*htlPIF* double layer and treatment with HCl leads to a slight blue-shift (~3 nm) of the emission. Besides that, the overall stability of the photoluminescence spectrum was good. Thermal treatment, which did not harm the photoluminescence spectrum for temperatures up to 200°C under argon was already described in section 5.2.2. The development of a broad emission peaking at 590 nm was observed for annealing under ambient air. Since only high bake out temperatures lead to a non-dissolving film for subsequent deposited layers, its chemical stability at these temperatures is an ultimate requirement for PLED applications. Also its increased stability to acids is a necessary demand, because this layer is in contact with PEDOT:PSS.

7 Operational stability of PLED devices

This chapter deals with the stability of *homoPIF*, *coPIF-1* and *coPIF-2* with respect to humidity and oxygen in PLED devices. The idea was to operate the devices in a nitrogen atmosphere with defined amounts of oxygen or humidity. Due to their molecular size, oxygen and water can easily diffuse under and via pinholes through the metal cathodes into the polymer films.⁶ The experimental setup is described in the next section.

7.1 Adopted PLED design and experimental methodology

To ensure an exclusive interaction of oxygen or humidity with the active layer (*homoPIF*, *coPIF-1* or *coPIF-2*), a special device architecture was chosen⁶⁴:

- Due to the known strong interactions of calcium with oxygen and water, the top electrode of the devices was made of aluminum solely.
- To enhance diffusion into the active area, the top electrode of each device consisted of four equidistant 150 μm wide and 70 nm thick aluminum strips (Figure 7.1).
- No additional electron or hole transporting layers were used to exclude any possible additional interactions.

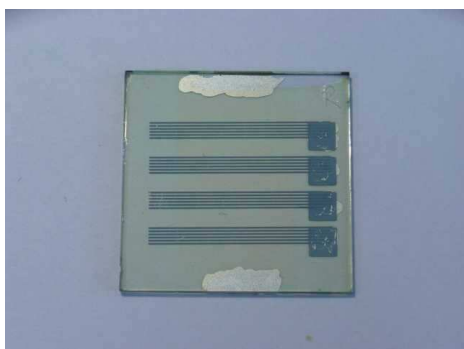




Figure 7.1: Top left: Ready made device; Top right: Measurement cell with gas in and outlet; Bottom left: Gas mixing and humidity measurement setup; Bottom right: Measurement cell with a rack for the fiber optics to the detector.

Defined atmospheres were produced with a gas mixing and humidity measurement plant (developed at the NTC Weiz Forschungsgesellschaft mbH⁶⁵) and applied to a special measurement cell with gas in- and outlet (Figure 7.1).

The actual measurement started with a reference measurement under argon atmosphere followed by a change of the atmosphere for a certain time (cycle 1). Subsequently the device was stored under high vacuum ($< 10^{-5}$ mbar) for 60 minutes to reduce possibly diffused oxygen or water, followed by a second cycle. In order to minimize operational device degradation, the PLED was switched off between the individual steps. Furthermore, a special rack (Figure 7.1, bottom right) ensured that the position of the fiber optics to the detector did not change during or between the cycles. This precaution allowed the comparison of the detected emission intensities.

7.2 Stability of homoPIF

Figure 7.2 shows the electroluminescence spectra of a *homoPIF* device under argon and under artificial air (22% O₂ and 78% N₂) during cycle 1 and cycle 2.

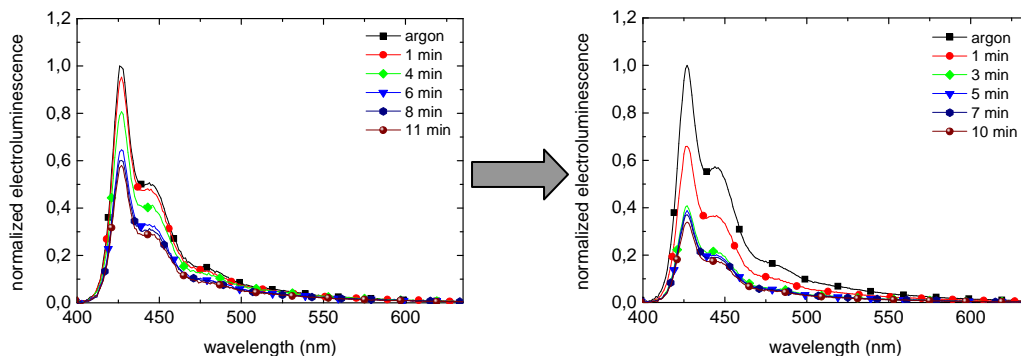


Figure 7.2: Electroluminescence spectra of *homoPIF* recorded under argon (black lines) and subsequently under artificial air after certain times (see legend). Cycle 2 (right) was recorded after a 1 hour vacuum storage.

A spectrally stable decrease to $\sim 57\%$ of the emitted intensity was found during cycle 1. During cycle 2 the intensity decrease was much faster: After 10 minutes in artificial atmosphere $\sim 34\%$ remained. These increased effects can be assigned to the formation of non-emissive dark spots.

7.3 Stability of *coPIF-1*

Find the electroluminescence spectra of *coPIF-1* recorded under argon and under artificial air (22% O_2 and 78% N_2) after certain times in figure 7.3.

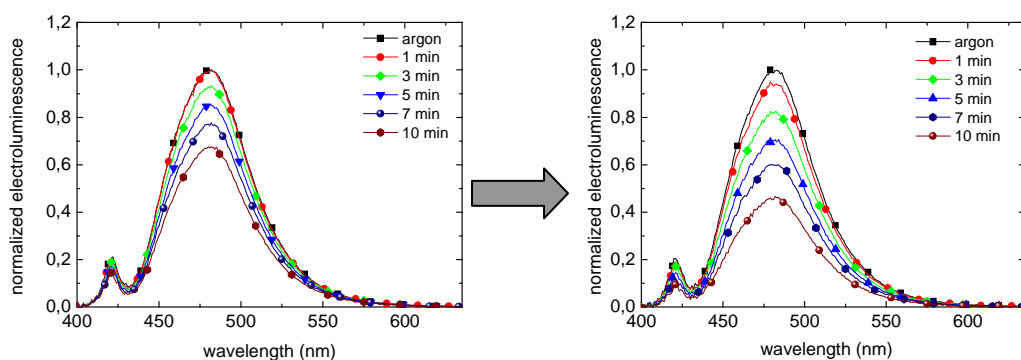


Figure 7.3: Electroluminescence spectra of *coPIF-1* recorded under argon (black lines) and subsequently under artificial air after certain times (see legend). Cycle 2 (right) was recorded after a 1 hour vacuum storage.

A spectrally stable decrease to ~68% compared to the maximum intensity was found during cycle 1. The decrease in cycle 2 was much faster and ~46% of the originally emitted intensity remained. This again can be ascribed to the formation of dark spots. In contrast to *homoPIF* and *coPIF-2*, the emitted spectrum strongly differs from the photoluminescence measurement. Here, the emissions maximum can be found around 483 nm. A second peak appears at 428 nm.

7.4 Stability of coPIF-2

As described in Chapter 6 *coPIF-2* had the worst spectral stability leading to extended investigations of this polymer. Besides longer lasting interaction times (20 minutes), an additional humidity influence was investigated. Moreover, a reference measurement under pure nitrogen atmosphere was performed.

Oxygen Interaction

An artificial atmosphere consisting of 22% O₂ and 78% N₂ was used. The results can be found in figure 7.4.

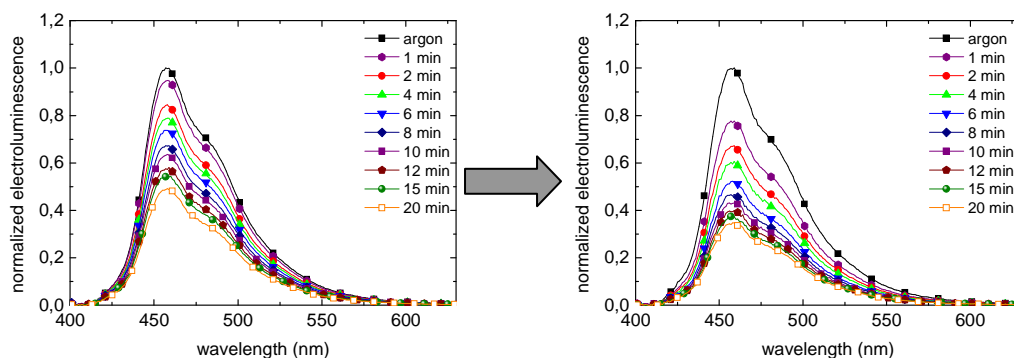


Figure 7.4: Electroluminescence spectra of *coPIF-2* recorded under argon (black lines) and subsequently under artificial air after certain times (see legend). Cycle 2 (right) was recorded after a 1 hour vacuum storage.

During cycle 1 a spectrally stable luminescence intensity decrease to 55% was found. The second cycle led to a faster reduction of the emitted intensity. After 20 minutes, 34% remained. Again, the spectrum was also stable during cycle 2.

Humidity interaction

A humidified (20% relative humidity) nitrogen carrier gas was used as artificial atmosphere in this experiment. Find the results in figure 7.5.

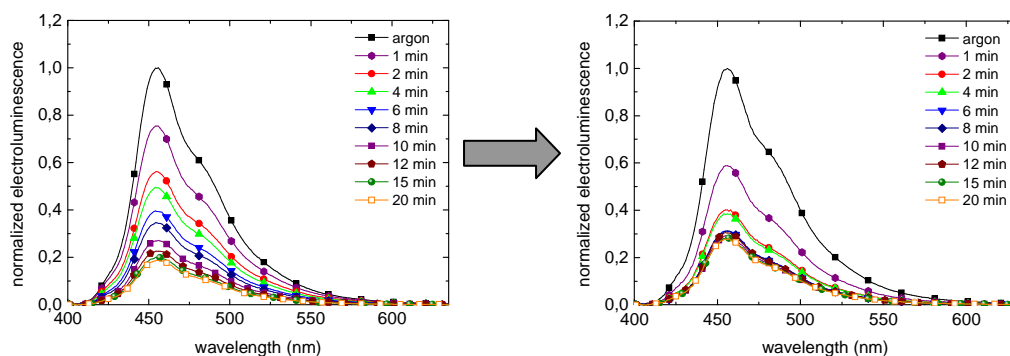


Figure 7.5: Electroluminescence spectra of *coPIF-2* recorded in argon (black lines) and in artificial humidified atmosphere after certain times (see legend). Cycle 2 (right) was recorded after a 1 hour vacuum storage.

The continuous exposition to humidity led to a spectrally stable decrease of the emitted intensity to $\sim 20\%$. During cycle 2, the emitted intensity decreased much faster and $\sim 30\%$ remained.

Reference measurement

To exclude possible influences of the device operation itself, measurements under argon and subsequently under pure nitrogen atmosphere instead of oxygen or humidified atmosphere were carried out. Figure 7.6 shows the results for both cycles.

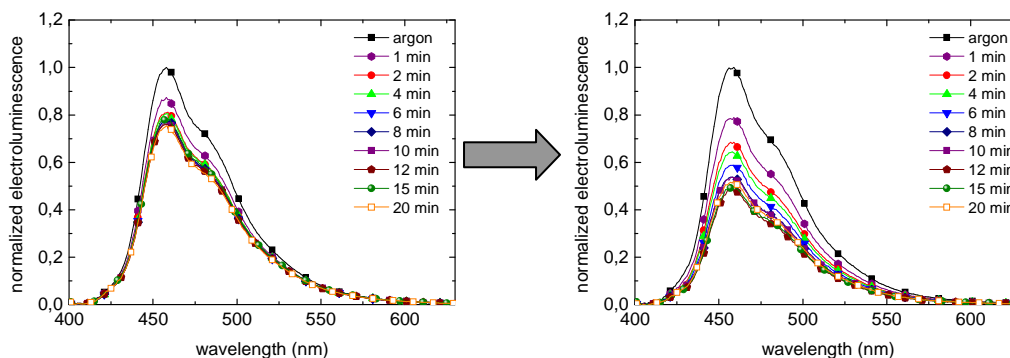


Figure 7.6: Electroluminescence spectra of *coPIF-2* recorded under argon (black lines) and subsequently under nitrogen atmosphere after certain times (see legend). Cycle 2 (right) was recorded after a 1 hour vacuum storage.

Only a limited decrease to ~80% of the originally emitted intensity was found during cycle 1 and to ~50% during cycle 2, respectively. This clearly shows that the device operation under inert atmosphere or the switch on/switch off events had only very limited influence.

7.5 Summary and discussion

All devices showed a similar behavior. Find an exemplary discussion on *coPIF-2* in this section. The intensity over time characteristics of *coPIF-2* for pure nitrogen atmosphere, oxygen atmosphere and humidified atmosphere are depicted in figure 7.7. The results of all experiments showed a very similar picture:

- Cycle 1: Spectrally stable decrease of the emitted electroluminescence intensity.
- High vacuum storage: At least partial recovery of the original emitted intensity.
- Cycle 2: Faster and stronger decrease of the emitted EL intensity.

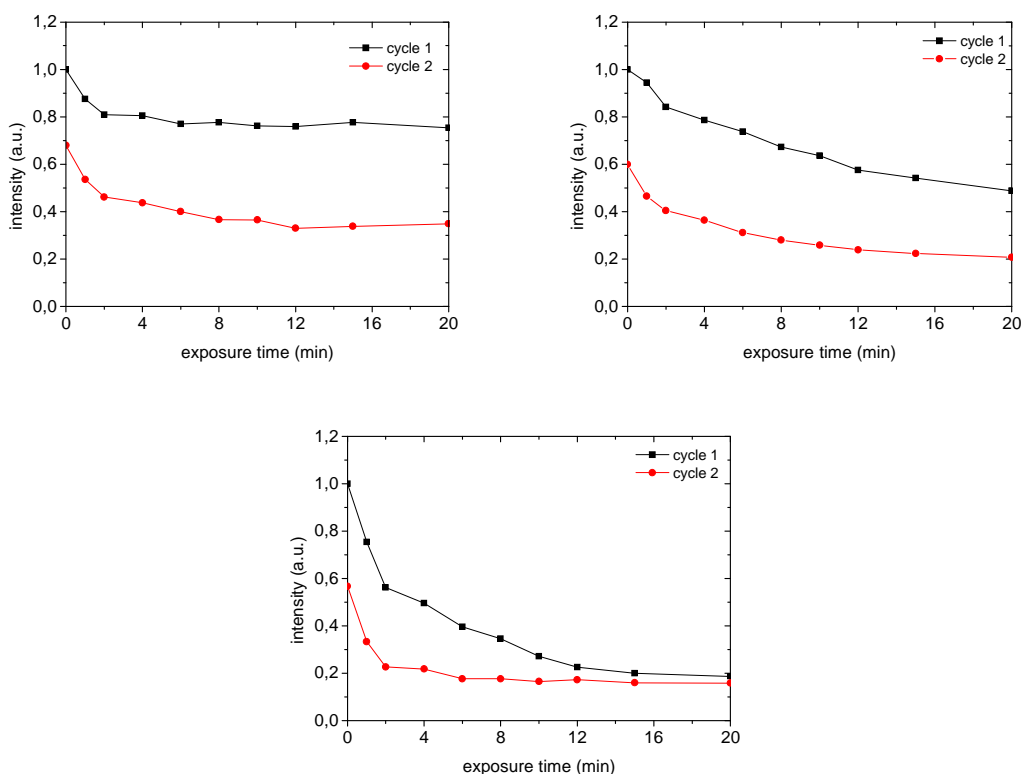


Figure 7.7: Intensity over time of *coPIF-2*. Left: Reference measurements under nitrogen atmosphere. Right: Influence of artificial air (22% O₂ and 78% N₂) onto the emitted EL intensity. Bottom: Influence of humidified nitrogen (20% relative humidity) onto the emitted EL intensity. (Black curves/squares: cycle 1; Red curves/circles: cycle 2)

Reference measurements in pure nitrogen revealed only a very limited decrease of the emitted intensity especially during cycle 1. Therefore, the investigated effects cannot be explained just by device degradation during operation. Also the formation of non-emissive dark spots due to cathode delamination cannot be responsible entirely because of the fact that the emitted intensity partly restores after high vacuum storage. However, the faster decrease of the emitted electroluminescence intensity during a second cycle can be assigned to an enhanced diffusion through pinholes in the cathode and dark spot generation.

This decrease of the emission intensity can be observed for phosphorescent materials⁶⁶ as well as for fluorescent polymers like in this case. However, the underlying mechanism may be of fundamental difference. As described in section 2.4, phosphorescence arises from the recombination of a triplet exciton. Those states usually have a long lifetime in the range of microseconds to seconds. Quenching can only occur in the case of molecular contact between diffused oxygen and the excited polymer within this lifetime. In contrast to phosphorescence, singlet excitons in fluorescent materials have a rather short lifetime usually in the range of picoseconds to a few nanoseconds which is orders of magnitude smaller than the lifetime of triplet excitons. Thus the quenching of triplet excitons seems to be much more likely.

In addition to that, only ground state oxygen acts as quencher. It is known that excited oxygen has a lifetime of several microseconds depending on the matrix material. Repeated quenching is only possible if the excited oxygen molecule has returned to its ground state again. Due to the extensive lifetime difference between an excited singlet state of a polymer and the oxygen molecule, which is at least four orders of magnitude, efficient quenching of singlet excitons seems from this point of view unlikely.

The question, whether there is sufficient oxygen available in the polymer film to explain the strong decrease of EL-intensity, is not fully answered so far. However, there might be other mechanisms responsible for the intensity decrease in fluorescent materials. Besides static quenching, possible candidates would be any polaron-oxygen/humidity interaction.

8 PLED device optimization with respect to their efficiency

Besides the study of different environmental influences, different PLED architectures with respect to the devices efficiency were realized. All materials, *homoPIF* (**1**), *coPIF-1* (**2**) and *coPIF-2* (**3**) were characterized in an basic PLED single layer structure: ITO/PEDOT:PSS/**1, 2, 3**/Ca/Al. In a next step, charge transporting layers - *htlPIF* and TPBi - were introduced: ITO/PEDOT:PSS/*htlPIF*/**1, 2, 3**/TPBi/Ca/Al. The inherent problem in the preparation of solution processed multi-layer PLEDs concerning the dissolving of subjacent layers was already described in chapter 5.2.2. After annealing at 200°C followed by a treatment with pure solvent no dissolving of the beneath coated *htlPIF* layer was found. Furthermore, the photophysical properties (PL, absorbance) remained unchanged. To elucidate the observed spectral characteristics, additionally devices with *htlPIF*+**1, 2, 3** 1:10 blends as active layer were fabricated: ITO/PEDOT:PSS/*htlPIF*+**1, 2, 3**/TPBi/Ca/Al. Further on, the absence of PEDOT:PSS onto the emission characteristics was examined in an ITO/*homoPIF*/Ca/Al PLED structure. As a first step, devices fabricated from *htlPIF* and TPBi were investigated.

All layers were prepared using following parameters (if not stated otherwise):

Table 8.1: PLED device preparation parameters

	Layer thickness	Annealing parameters
PEDOT:PSS	60 nm	120°C for 1 h
htlPIF	20 nm	70°C / 200°C for 1 h
Active layer - PIF	45 nm / 150 nm	70°C for 1 h
TPBi	10 nm; Rate: 0.2 nm/s	-
Ca	10 nm; Rate: 0.2 nm/s	-
Al	100 nm; Rate: 1 nm/s	-

8.1 *htlPIF* and TPBi-only device

As shown in section 5.2, *htlPIF* exhibits good photophysical properties: High photoluminescence quantum yield, good thermal stability and blue photoluminescence emission. Besides that, its band gap is smaller than that of *homoPIF* and *coPIF-1* which may lead to a situation where holes are efficiently injected into the active layer, but electrons are not blocked at the *htlPIF/1, 2, 3* interface. Reason enough to investigate *htlPIF*'s performance in a PLED without any actual active material. A ITO/PEDOT:PSS/100 nm *htlPIF*/TPBi/Ca/Al device was prepared. The current - voltage - luminance characteristics as well as the electroluminescence spectrum are depicted in figure 8.1. The results are summarized in table 8.2.

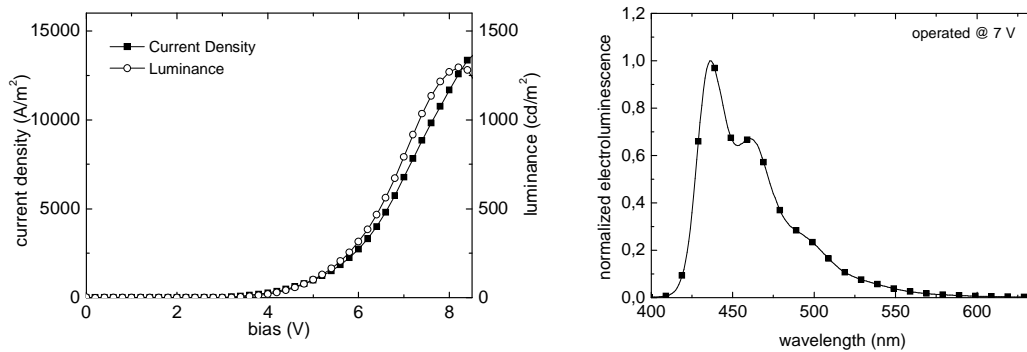


Figure 8.1: Voltage-current-luminance characteristic (left) and electroluminescence spectrum (right) of an ITO/PEDOT:PSS/100 nm *htlPIF*/TPBi/Ca/Al device.

Table 8.2: Key results of an ITO/PEDOT:PSS/100 nm *htlPIF*/TPBi/Ca/Al device.

onset	max. luminance	max. efficiency	peak maximum	CIE1931
3.2 V	1293 cd/m ² @8 V	0.12 cd/A @7 V	437 nm	x = 0.151 y = 0.085

The electroluminescence emission exhibits blue emission (CIE1931 $x = 0.151$; $y = 0.085$) with a maximum at 437 nm. The high current density up to 14000 A/m² is the result of the increased hole transport in the device. Despite luminance values up to 1300 cd/m², the efficiency of 0.12 cd/A is quite low.

8.2 PLEDs based on homoPIF

Single layer, multi layer and blend systems with *homoPIF* are presented in the following. To investigate the influence of PEDOT:PSS on the EL emission spectrum, an additional device structure without PEDOT:PSS will be shown.

8.2.1 ITO/PEDOT:PSS/150 nm homoPIF/Ca/Al

This basic single layer configuration led to poor efficiencies and luminance values (see figure 8.2 and table 8.3): A high current density up to 20000 A/m^2 was found while the maximum luminance with 290 cd/m^2 was low. Consequently the devices showed poor efficiency in the range of 0.025 cd/A . However, blue electroluminescence emission was found (CIE1931 $x = 0.173$; $y = 0.082$) with a maximum at 428 nm and a vibronic feature around 446 nm .

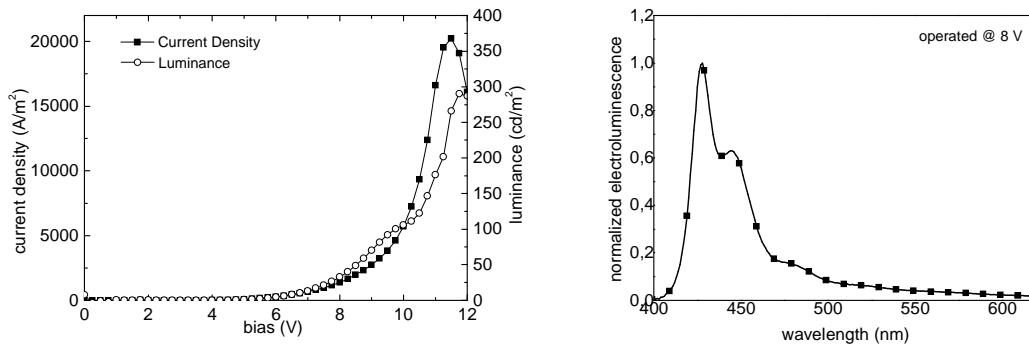


Figure 8.2: Voltage-current-luminance characteristic (left) and electroluminescence spectrum (right) of an ITO/PEDOT:PSS/150 nm *homoPIF*/Ca/Al device.

Table 8.3: Key results of an ITO/PEDOT:PSS/150 nm *homoPIF*/Ca/Al device.

onset	max. luminance	max. efficiency	peak maximum	CIE1931
4.0 V	290 cd/m^2 @11 V	0.025 cd/A @9 V	428 nm	$x = 0.173$ $y = 0.082$

The influence of PEDOT:PSS

The results in Chapter 6.3 revealed no distinct influence of PEDOT:PSS onto the photoluminescence spectrum of *homoPIF*. To investigate a possible effect on the electroluminescence spectrum, devices with and without a PEDOT:PSS layer and with different active layer thicknesses were fabricated. The active layer thickness in one case was ~45 nm and in the second ~150 nm. Deviations in the layer thicknesses due to the different wetting of the subjacent material (ITO solely or ITO/PEDOT:PSS) was low (< 5%) and can be neglected. The resulting EL spectra are shown in figure 8.3.

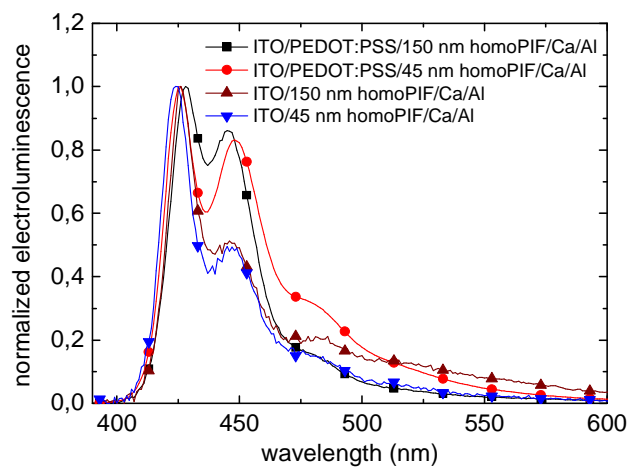


Figure 8.3: Electroluminescence spectra of devices with and without a PEDOT:PSS layer and with different active layer thicknesses (see legend).

Apart from the poor performance of the devices without PEDOT:PSS layer, they show a less pronounced vibronic transition. One explanation of the investigated effect is a different location of the charge carrier recombination zone and the light out coupling (Figure 8.4). In devices without PEDOT:PSS and with a calcium cathode, the recombination zone is expected to be near the ITO/OSC interface. Therefore a fraction of the emitted light can leave the device without passing the active layer. Devices with PEDOT:PSS layer show better hole-injection. Although the recombination zone is still expected to be near the anode^{67,68}, it might be broadened and shifted towards the bulk. Now parts of the emitted photons have to pass parts of the active layer and are therefore possibly prone to self-absorption.

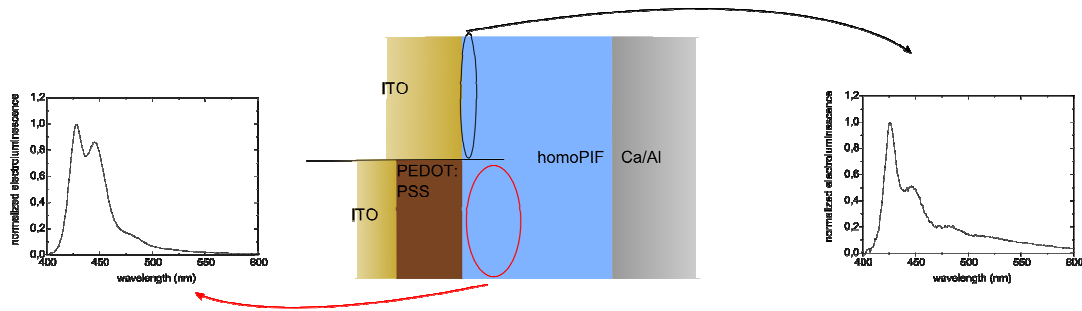


Figure 8.4: Proposed location of the charge carrier recombination zone and the corresponding EL spectra.

However, this would require that the recombination zone for the two devices with different (45 nm and 150 nm) active layer thicknesses and with PEDOT:PSS is located exactly at the same position within the device. Further experiments on this topic, especially with different cathode materials (e.g. Ag, Al) and electron transporters, are suggested.

8.2.2 ITO/PEDOT:PSS/htPIF/homoPIF/TPBi/Ca/Al

As expected, the ITO/PEDOT:PSS/htPIF/homoPIF/TPBi/Ca/Al configuration showed much better performance (Figure 8.5, Table 8.4). Compared to the *homoPIF* single-layer device, the maximum luminance of 11000 cd/m² increased about 37-fold, the maximum efficiency increased ~48-fold. The electroluminescence emission appears red-shifted with a maximum at 442 nm and a shoulder around 464 nm (CIE1931 $x = 0.149$; $y = 0.097$).

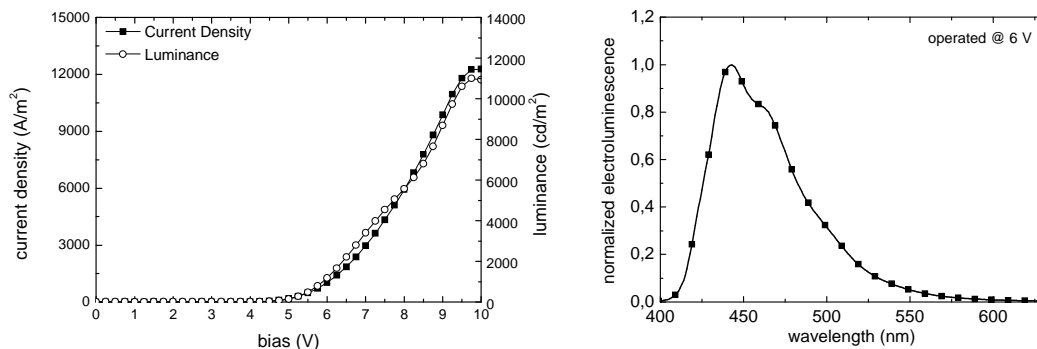


Figure 8.5: Voltage-current-luminance characteristic (left) and electroluminescence spectrum (right) of an ITO/PEDOT:PSS/20 nm htPIF/45 nm homoPIF/TPBi/Ca/Al device.

Table 8.4: Key results of an ITO/PEDOT:PSS/20 nm *htlPIF*/45 nm *homoPIF*/TPBi/Ca/Al device.

onset	max. luminance	max. efficiency	peak maximum	CIE1931
4.1 V	11004 cd/m ² @10 V	1.19 cd/A @6.5 V	442 nm	x = 0.149 y = 0.097

The spectrum can be attributed neither to *htlPIF* nor to *homoPIF* solely. A corporate emission of the two polymers seems possible. This would require an at least partial blending of *htlPIF* and *homoPIF* at their interface.

8.2.3 ITO/PEDOT:PSS/*htlPIF*+*homoPIF*/TPBi/Ca/Al

In order to investigate the origin of the electroluminescence spectrum in figure 8.5, a device with a *htlPIF*/*homoPIF* blend was fabricated. *htlPIF* and *homoPIF* were directly blended in solution with a ratio of *htlPIF*:*homoPIF* 1:10. The voltage-current density-luminance characteristic as well as the electroluminescence spectrum are depicted figure 8.6, a summary of the key results is presented table 8.5.

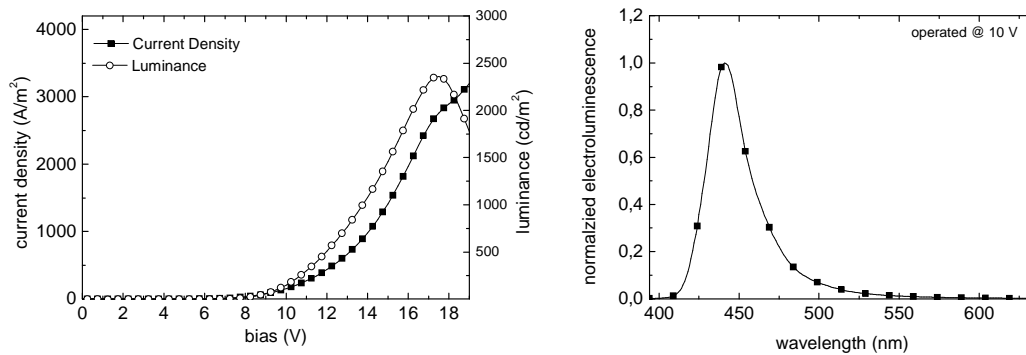

 Figure 8.6: Voltage-current-luminance characteristic (left) and electroluminescence spectrum (right) of an ITO/PEDOT:PSS/*htlPIF*+*homoPIF* 1:10/TPBi/Ca/Al device.

 Table 8.5: Key results of an ITO/PEDOT:PSS/*htlPIF*+*homoPIF* 1:10/TPBi/Ca/Al device.

onset	max. luminance	max. efficiency	peak maximum	CIE1931
8.6 V	2359 cd/m ² @17 V	1.17 cd/A @12 V	441 nm	x = 0.156 y = 0.044

Compared to the layered device, the onset voltage is more than doubled in this configuration and the current density was low. Also the observed maximum luminance de-

creased significantly by a factor of ~ 4 . The electroluminescence spectrum exhibits a narrow peak with a maximum at 441 nm.

8.2.4 Summary and discussion

Devices based on pristine poly(indenofluorene) *homoPIF* were fabricated in a single-layer structure, in a multi-layer structure with *htlPIF* as well as in a polymer blend system with *htlPIF*. Further on, the influence of the PEDOT:PSS layer on the emission characteristic was investigated. The latter led to a distinct difference - devices with PEDOT:PSS showed an enhanced second maximum. It seems that two mechanisms can be responsible for that. First, a shift of the recombination zone towards the bulk and thus increased self-absorption. Second, spectral changes induced by the acidic character of PEDOT:PSS. Further experiments are necessary for a complete explanation.

Table 8.6 summarizes the key results of the devices. Single-layer devices showed a comparatively bad performance. The implementation of *htlPIF* and TPBi to the system boosted device luminance and efficiency from rather low values to good results.

Table 8.6: Key results of the *homoPIF* based PLED devices.

	onset	max. luminance	max. efficiency	peak maximum	CIE1931
Single-layer	4.0 V	290 cd/m ² @11 V	0.025 cd/A @9 V	428 nm	x = 0.173 y = 0.082
Multi-layer	4.1 V	11004 cd/m ² @10 V	1.19 cd/A @6.5 V	442 nm	x = 0.149 y = 0.097
Blend	8.6 V	2359 cd/m ² @17 V	1.17 cd/A @12 V	441 nm	x = 0.156 y = 0.044

However, a spectral shift of the spectra obtained from multilayer and blend device configuration to a lighter blue region, which cannot be assigned to *htlPIF* or *homoPIF*, was observed. To elucidate the origin of the spectrum, devices with a *htlPIF+homoPIF* blend as active layer were fabricated. This led to a narrow emission characteristic, peaking in the same region like the multi-layer PLED. The spectra of the devices as well as the spectrum of the *htlPIF*-only device can be found in figure 8.7.

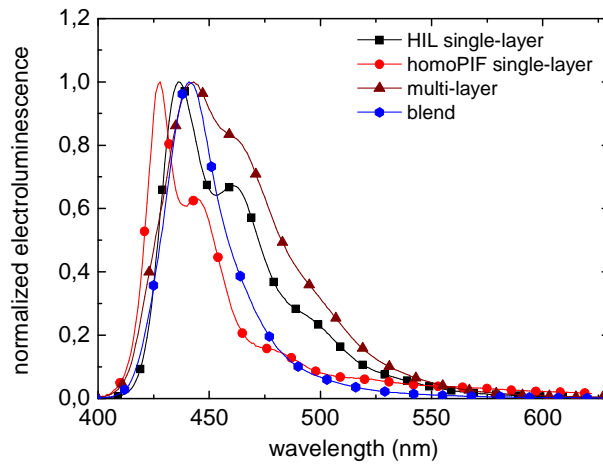


Figure 8.7: Comparison of the electroluminescence spectra of *htlPIF*, *homoPIF*, *htlPIF/homoPIF* multi-layer and *htlPIF+homoPIF* blend PLEDs.

The presented spectra indicate at least a partial blending of *htlPIF* and *homoPIF* at the interface. Also, parts of the charge carrier recombination zone might be located in or very close to the *htlPIF* layer leading to the observed broadenings and shifts.

8.3 PLEDs based on coPIF-1

Basically *coPIF-1* has a chemical structure based on *homoPIF* and additional a small amount of triphenylamine based units. Therefore, an increased efficiency due to its better hole transporting properties can be expected. Like in the previous chapter, a single-layer device, a multi-layer device and a blend device were prepared.

8.3.1 ITO/PEDOT:PSS/150 nm coPIF-1/Ca/Al

The basic ITO/PEDOT:PSS/coPIF-1/Ca/Al setup led to luminance values as high as 947 cd/m^2 (at 17.6 V). This is a clear improvement to the *homoPIF* single-layer PLED. Efficiencies are still low around 0.11 cd/A (at 14.2 V). The obtained electroluminescence emission was deep blue with its maximum at 428 nm (CIE1931: $x = 0,166$; $y = 0,074$). The results are presented in figure 8.8 and summarized in table 8.7.

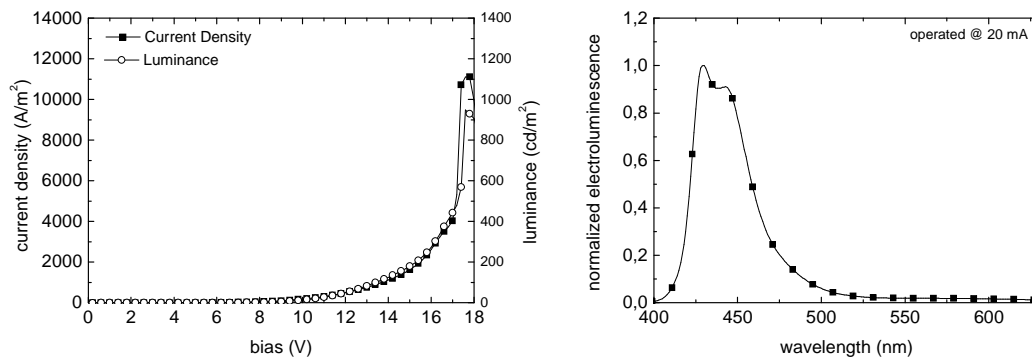


Figure 8.8: Voltage-current-luminance characteristic (left) and electroluminescence spectrum (right) of an ITO/PEDOT:PSS/*coPIF-1*/Ca/Al device.

Table 8.7: Key results of an ITO/PEDOT:PSS/*coPIF-1*/Ca/Al device.

onset	max. luminance	max. efficiency	peak maximum	CIE1931
7.5 V	947 cd/m^2 @ 17.6 V	0.11 cd/A @ 14.2 V	428 nm	$x = 0.166$ $y = 0.074$

8.3.2 ITO/PEDOT:PSS/htlPIF/coPIF-1/TPBi/Ca/Al

The highest luminance value of 21173 cd/m² as well as a high efficiency with 3.25 cd/A were obtained from the ITO/PEDOT:PSS/htlPIF/coPIF-1/TPBi/Ca/Al device structure. A major drawback of this configuration was the significant red-shift of the emission compared to the single-layer device. The EL emission shows a broad peak centered around 465 nm (CIE1931 $x = 0.151$; $y = 0.183$).

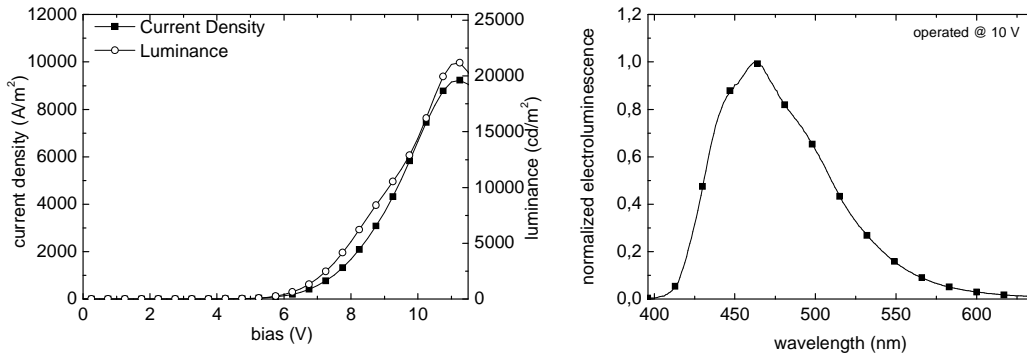


Figure 8.9: Voltage-current-luminance characteristic (left) and electroluminescence spectrum (right) of an ITO/PEDOT:PSS/20 nm htlPIF/45 nm coPIF-1/TPBi/Ca/Al device.

Table 8.8: Key results of an ITO/PEDOT:PSS/20 nm htlPIF/45 nm coPIF-1/TPBi/Ca/Al device.

onset	max. luminance	max. efficiency	peak maximum	CIE1931
4.7 V	21173 cd/m ² @ 11.25 V	3.25 cd/A @ 6.75 V	465 nm	$x = 0.151$ $y = 0.183$

Again, the observed electroluminescence emission characteristic can be assigned neither to *coPIF-1* ($\lambda_{\max} = 428$ nm) nor to *htlPIF* ($\lambda_{\max} = 437$ nm) and at least partial blending at their interface can be supposed.

8.3.3 ITO/PEDOT:PSS/*htlPIF*+*coPIF*-1/TPBi/Ca/Al

In order to verify the supposed blending at the interface in the previous chapter, *htlPIF* and *coPIF*-1 were blended directly in solution with a ration of 1:10 and used as active layer for this PLED (Figure 8.1, Table 8.9).

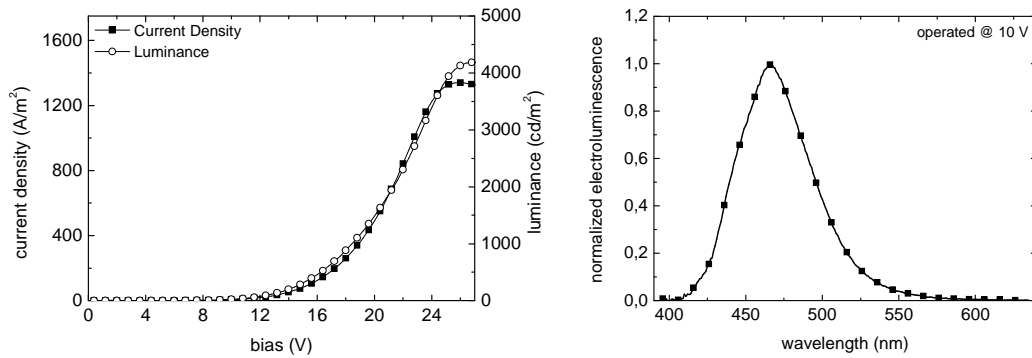


Figure 8.10: Voltage-current-luminance characteristic (left) and electroluminescence spectrum (right) of an ITO/PEDOT:PSS/*htlPIF*+*coPIF*-1 1:10/TPBi/Ca/Al device.

Table 8.9: Key results of an ITO/PEDOT:PSS/*htlPIF*+ *coPIF*-1 1:10/TPBi/Ca/Al device.

onset	max. luminance	max. efficiency	peak maximum	CIE1931
8.6 V	4187 cd/m ² @26.8 V	4.06 cd/A @8.4 V	467 nm	x = 0.135 y = 0.121

With 4.06 cd/A, the best measured device efficiency was observed from this structure, while the achieved maximum luminance was only $\sim 1/5$ of the corresponding luminance of the layered PLED. Also the onset voltage and the driving voltages are higher than before. The electroluminescence spectrum shows a narrower and unstructured maximum peaking at 467 nm, which is nearly at the same wavelength as for the layered device.

8.3.4 Summary and discussion

For devices based on *coPIF*-1 a better performance than for *homoPIF* was expected due to its increased hole transporting properties. A single-layer, a multi-layer with *htlPIF* and a blend device were prepared. The summary of the obtained results can be found in table 8.10.

Table 8.10: Key results of the coPIF-1 based PLED devices.

	onset	max. luminance	max. efficiency	peak max.	CIE1931
Single-layer	7.5 V	947 cd/m ² @17.6 V	0.11 cd/A @14.2 V	428 nm	x = 0.166 y = 0.074
Multi-layer	4.7 V	21173 cd/m ² @11.25 V	3.25 cd/A @6.75 V	465 nm	x = 0.151 y = 0.183
Blend	8.6 V	4187 cd/m ² @26.8 V	4.06 cd/A @8.4 V	467 nm	x = 0.135 y = 0.121

The single-layer structure showed a deep blue emission spectrum but low luminance values and efficiencies. The multi-layer PLED gave the highest luminance values within this work as well as good efficiencies. However, the emission maximum was significantly shifted to a lower energy region. This should be kept in mind when interpreting luminance and efficiency, because of the non-linear relationship between emission color and luminance.⁶⁹ Blend devices showed the best efficiencies but also a red-shifted emission spectrum compared to single- and multi-layer device. The spectra of the devices as well as the spectrum of the *htlPIF*-device can found in figure 8.11.

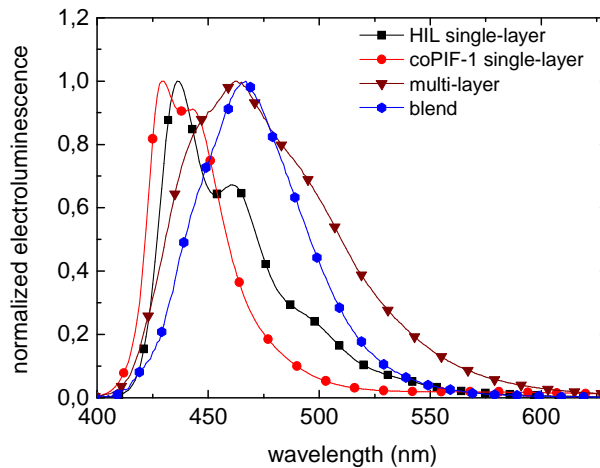


Figure 8.11: Comparison of the electroluminescence spectra of *htlPIF*, *coPIF-1*, *htlPIF/coPIF-1* multi-layer and *htlPIF+coPIF-1* blend PLEDs.

The shape of the multi-layer and the blend spectrum, especially their common emission maximum strongly indicate that the electroluminescence spectrum of the multi-layer device arises from partial blending at the *htlPIF/coPIF-1* interface. Also the recombina-

tion zone can be assumed to be around the interface. However, the exact nature of the emission spectrum remains unclear.

8.4 PLEDs based on coPIF-2

Additional to the amine units of *coPIF-1*, phenylene-vinylene units are implemented in, *coPIF-2*. Photoluminescence investigations already showed that these units are efficient emitters but were found to be unstable with respect to ambient and acidic influences (Chapter 6). Device structures equal to the previously presented were fabricated.

8.4.1 ITO/PEDOT:PSS/150 nm coPIF-2/Ca/Al

Devices with a *coPIF-2* single layer showed an emission maximum at 446 nm and a shoulder at 426 nm, with a maximum luminance of 938 cd/m² and a maximum efficiency of 0.2 cd/A. A high onset voltage around 12 V was measured. The results are presented in figure 8.12 and summarized in table 8.11.

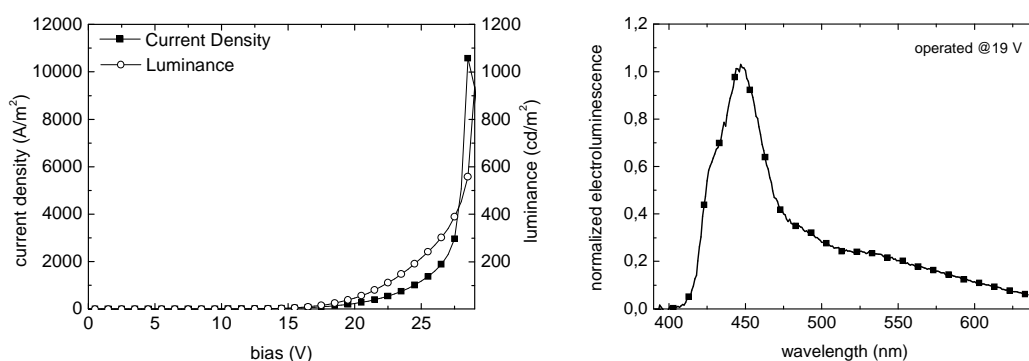


Figure 8.12: Voltage-current-luminance characteristic (left) and electroluminescence spectrum of an ITO/PEDOT:PSS/*coPIF-2*/Ca/Al device.

Table 8.11: Key results of an ITO/PEDOT:PSS/150 nm *coPIF-2*/Ca/Al device.

onset	max. luminance	max. efficiency	peak maximum	CIE1931
12 V	938 cd/m ² @29 V	0.2 cd/A @22 V	446 nm	x = 0.205 y = 0.187

8.4.2 ITO/PEDOT:PSS/htlPIF/*coPIF-2*/TPBi/Ca/Al

The ITO/PEDOT:PSS/htlPIF/*coPIF-2*/TPBi/Ca/Al multi-layer device structure showed strongly improved device properties compared to the single-layer architecture. Lumi-

nance values up to 17000 cd/m^2 were measured. The maximum efficiency of 2.31 cd/A was measured at 6.5 V . As for *homoPIF* and *coPIF-1* the broad and mostly structureless electroluminescence emission (CIE1931: $x = 0,142$; $y = 0,151$) with a maximum at 460 nm is red-shifted by 14 nm compared to the single-layer device. Again, a blending at the interface can be a possible reason.

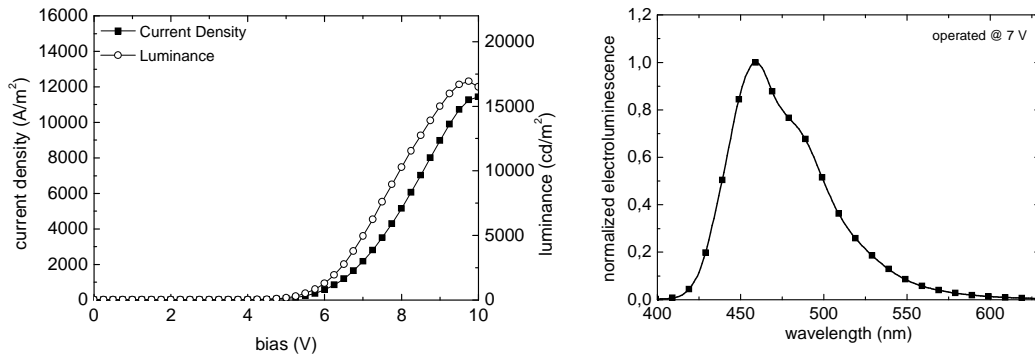


Figure 8.13: Voltage-current-luminance characteristic (left) and electroluminescence spectrum (right) of an ITO/PEDOT:PSS/20 nm *htPIF*/45 nm *coPIF-2*/TPBi/Ca/Al device.

Table 8.12: Key results of an ITO/PEDOT:PSS/20 nm *htPIF*/45 nm *coPIF-2*/TPBi/Ca/Al device.

onset	max. luminance	max. efficiency	peak maximum	CIE1931
12 V	16927 cd/m^2 @9.75 V	2.31 cd/A @6.5 V	460 nm	$x = 0.142$ $y = 0.151$

8.4.3 ITO/PEDOT:PSS/*htPIF*+*coPIF-2*/TPBi/Ca/Al

As in the case of *homoPIF* and *coPIF-1*, the device structure with a *htPIF*+*coPIF-2* 1:10 blend as active layer was fabricated to investigate and to compare the nature of the electroluminescence spectrum with multi-layer devices. The results are presented in figure 8.14 and in table 8.13.

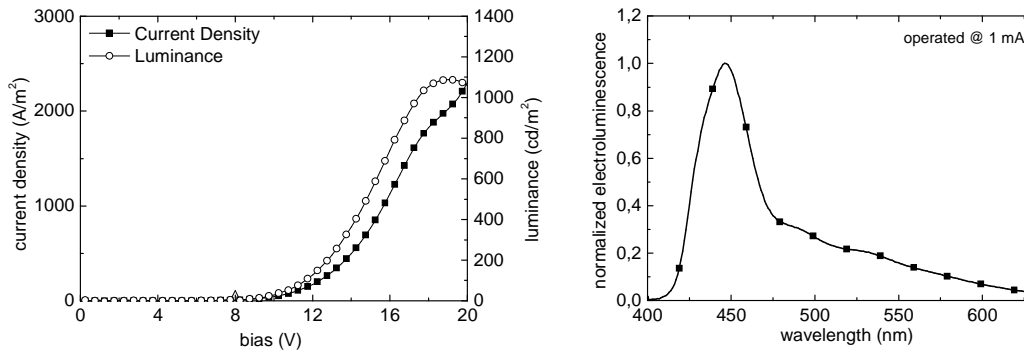


Figure 8.14: Voltage-current-luminance characteristic (left) and electroluminescence spectrum (right) of an ITO/PEDOT:PSS/hlPIF+coPIF-2 1:10/TPBi/Ca/Al device.

Table 8.13: Key results of an ITO/PEDOT:PSS/hlPIF+coPIF-2 1:10/TPBi/Ca/Al device.

onset	max. luminance	max. efficiency	peak maximum	CIE1931
7 V	1087 cd/m ² @19 V	0.74 cd/A @13 V	446 nm	x = 0.187 y = 0.161

Compared to the multi-layer device, the luminance and the device efficiency were much lower. Its emission characteristics, with a maximum at around 446 nm, was similar to the emission spectrum of the *coPIF-2* single-layer devices.

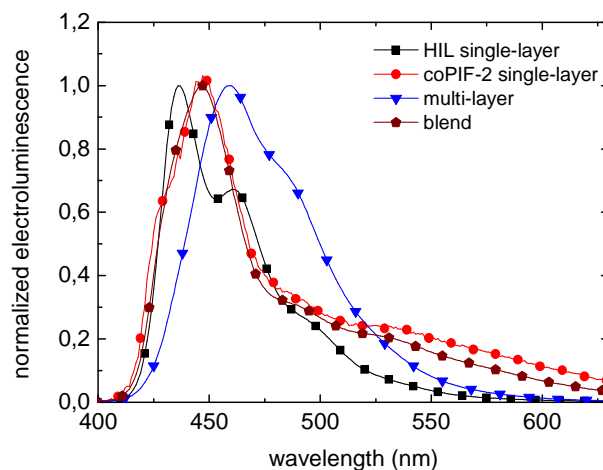
8.4.4 Summary and discussion

As for *homoPIF* and *coPIF-1*, the single layer device showed the worst performance with respect to maximum luminance and to maximum efficiency. A strong increase of the obtained luminance and efficiencies was found for the multi-layer device. However, compared to the single-layer systems, a red-shift of 14 nm of the emission maximum was observed. Devices with a blend system as active layer again showed a lower maximum luminance and maximum efficiency. Find all results summarized in table 8.14.

Table 8.14: Key results of the *coPIF-2* based PLED devices.

	onset	max. luminance	max. efficiency	peak maximum	CIE1931
Single-layer	12 V	938 cd/m ² @29 V	0.2 cd/A @22 V	446 nm	x = 0.205 y = 0.187
Multi-layer	12 V	16927 cd/m ² @9.75 V	2.31 cd/A @6.5 V	460 nm	x = 0.142 y = 0.151
Blend	7 V	1087 cd/m ² @19 V	0.74 cd/A @13 V	446 nm	x = 0.187 y = 0.161

The spectra of all three different device structures as well as the spectrum of the *htlPIF*-only device structure can be found in figure 8.15. In strong contrast to the results of the *homoPIF* and *coPIF-1* PLEDs, here the emission spectrum of the single layer device and the emission of the blend device nearly overlap. A possible explanation to this overlap can be given by the picture of charge carrier movement towards energetically favorable states. Phenylene-vinylene units usually have a band gap lower in energy than that of poly(indenofluorene).⁷⁰ Since a lower band gap represents an energetically favorable position for charge carriers on *htlPIF* and *coPIF-2*, phenylene-vinylene units might act as trap and recombination occurs mostly at these units. Thus, the emitting species in both cases (*coPIF-2* single-layer devices & blend devices) are the phenylene-vinylene units, leading to nearly identical emission spectra.

Figure 8.15: Comparison of the electroluminescence spectra of *htlPIF*, *coPIF-2*, *htlPIF/coPIF-2* multi-layer and *htlPIF+coPIF-2* blend PLEDs

9 Conclusion

The scope of the presented master thesis was the photophysical and electrooptical characterization of poly(indenofluorene) based homo and copolymers. Chapter 4 presents the used experimental methodology, including a detailed description of an indirect method to measure the photoluminescence quantum yield for solutions. A careful calibration of the operated spectrofluorophotometer, which is an important requirement for this measurements, was successfully realized.

The basic photophysical investigations revealed mostly unstructured absorption spectra with a maximum around 400 nm for all three polymers. The emission is, however, strongly depended on the different chemical properties: *homoPIF* showed the expected poly(indenofluorene) emission similar to spectra reported in literature.¹⁵ A strong enhancement of the second maximum was found for *coPIF-1*. *coPIF-2* showed a red shifted emission maximum around 457 nm, which is apparently due to its phenylene-vinylene units which are considered to the emitting species.

Different approaches were made to investigate the stability of the materials with respect to thermal stress, UV-irradiation and acidic environments. A good spectral stability can be assigned to *homoPIF*, *coPIF-1* and *htlPIF*: Changes during all kinds of treatment were limited, but always related to a relative decrease of the emission maximum at 424 nm and to an increase of the relative emission between 480 nm and 600 nm. However, the observed effects were bigger for treatments under ambient conditions which clearly indicates oxygen or humidity induced effects. A possible explanation can be the related photosensitized production of singlet oxygen which might react with the polymer, thus leading to the spectral instabilities. The absolute emission intensities always decreased. The fact that no recovery of the intensity was measured after a 2 hour lasting HV storage leads to the exclusion of dynamic quenching as causing factor. The spectrum of *coPIF-2* showed another behavior during treatment - related to the emission maximum at 457 nm which is due to phenylene-vinylene emission, the shoulder at 424 nm developed to a pronounced peak which can be assigned to the deactivation of the phenylene-vinylene emission, whereas the PIF emission remains. A possible process occurring during thermal stress or UV irradiation is a dissociation of the emissive unit into non emissive aldehydes.^{59,60} The spectral changes in acidic environments may be

due to an electrophilic addition of the acid to the nucleophile carbon double bond of the vinylene unit.

The operational stability of PLED devices was investigated in chapter 7. Every tested device configuration showed the same behavior: Spectral stable electroluminescence intensity decrease when operated in artificial atmosphere (22% O₂ in N₂ or 20% relative humidity in N₂) and at least partial recovery of the emitted intensity after 1 h HV storage. In a second operation cycle the intensity decreased faster. These observations clearly indicate a dynamic process, however, its exact nature is not completely understood so far. Quenching by oxygen or water is more unlikely than for phosphorescent dyes due to their shorter excited state lifetimes and the long excited state lifetime of O₂.

The scope of Chapter 8 was the optimization of different PLED device structures with respect to the efficiency. The single layer configuration showed the worst efficiency and luminance for all three emitter materials. However, the obtained electroluminescence spectra were similar to the photoluminescence spectra. Additional electron and hole transport layers increased the highest luminance values as well as the efficiencies. The best results were obtained for *coPIF-1* with ~ 21100 cd/m² and 3.25 cd/A. Also, a red-shift compared to the single-layer devices was found. Due to the fact that devices with a *htlPIF+PIF* blend as active layer, showed similar electroluminescence spectra, the origin of this effect was assigned to a partial blending at the *htlPIF/PIF* interfacial region. This mutual dissolving of the used solvents points out the major problem of solution processed multi-layer PLEDs. To overcome this disadvantage, completely cross-linking hole transport materials or orthogonal solubility of the used polymers are desired. Various approaches towards the latter, such as the fabrication of structures using polymers with fluorinated and non-fluorinated side-chains, were pursued lately.⁷¹

Bibliography

- [1] H. Shirakawa, E. J. Louis, S. C. Gau, A. G. MacDiarmid, C. K. Chiang, C. R. Finger jr., Y. W. Park, A. J. Heeger, *Phys. Rev. Lett.* 1977, 39, 1098.
- [2] J. H. Burroughes, D. D. C. Bradley, A. R. Brown, R. N. Marks, K. Mackay, R. H. Friend, P. L. Burns, A. B. Holmes, *Nature* 1990, 347, 539.
- [3] S. Günes, H. Neugebauer, N. S. Sariciftci, *Chem. Rev.* 2007, 107, 1324.
- [4] F. Garnier, R. Hajlaoui, A. Yassar, P. Srivastava, *Science* 1994, 265, 1684.
- [5] H. C. Langowski, *Vakuum in Forschung und Praxis* 2002, 5, 297.
- [6] O. Miesbauer, M. Schmidt, H. C. Langowski, *Vakuum in Forschung und Praxis* 2008, 20, 32.
- [7] L. Pauling, *J. Am. Chem. Soc.* 1931, 53, 1367.
- [8] <http://wps.prenhall.com/>, 27.1.2010.
- [9] E. J. W. List, U. Scherf, *Handbook of conducting polymers* 3rd Edition, Chapter 5, CRC Press 2007.
- [10] M. Fukuda, K. Sawada, K. Yoshino, *J. Polym. Sci., Part A: Polym. Chem.* 1993, 31, 2465.
- [11] K.-T. Wong, Y.-Y. Chien, R.-T. Chen, C.-F. Wang, Y.-T. Lin, H.-H. Chiang, P.-Y. Hsieh, C.-C. Wu, C. H. Chou, Y. O. Su, G.-H. Lee, S.-M. Peng, *J. Am. Chem. Soc.* 2002, 124, 11576.
- [12] S. Setayesh, A. C. Grimsdale, T. Weil, V. Enkelmann, K. Müllen, F. Meghdadi, E. J. W. List, G. Leising, *J. Am. Chem. Soc.* 2001, 123, 946.
- [13] E. J. W. List, R. Guentner, P. Scandiucci de Freitas, U. Scherf, *Adv. Mater.* 2002, 14, 374.
- [14] S. Setayesh, D. Marsitzky, K. Müllen, *Macromol.* 2000, 33, 2016.
- [15] J. Jacob, J. Zhang, A. C. Grimsdale, K. Müllen, M. Gaal, E. J. W. List, *Macromol.* 2003, 36, 8240.
- [16] J. Jacob, S. Sax, T. Piok, E. J. W. List, A. C. Grimsdale, K. Müllen, *J. Am. Chem. Soc.* 2004, 126, 6987.
- [17] J. Jacob, S. Sax, M. Gaal, E. J. W. List, A. C. Grimsdale, K. Müllen, *Macromol.* 2005, 38, 9933.
- [18] S. Tasch, A. Niko, G. Leising, U. Scherf, *Appl. Phys. Lett.* 1998, 68, 1090.

- [19] S. F. Alvarado, P. F. Seidler, D. G. Lidzey, D. D. C. Bradley, *Phys. Rev. Lett.* 1998, 81, 1082.
- [20] C. Kittel, *Introduction to solid state physics*, 8th Edition, Wiley, 2005.
- [21] R. A. Marcus, *Rev. Mod. Phys.* 1993, 65, 3.
- [22] M. Kasha, *Discuss. Faraday Soc.* 1950, 9, 14
- [23] G. Heimel, M. Daghofer, J. Gierschner, E. J. W. List, A.C. Grimsdale, K. Müllen, D. Beljonne, J. L. Brédas, E. Zojer, *J. Chem. Phys.* 2005, 122, 054501.
- [24] B. Xu, S. Holdcroft, *Adv. Mater.* 1994, 6, 325.
- [25] R. Kersting, U. Lemmer, M. Deussen, H. J. Bakker, R. F. Mahrt, H. Kurz, V. I. Arkhipov, H. Bässler, E. O. Göbel, *Phys. Rev. Lett.* 1994, 73, 1440.
- [26] E. J. W. List, U. Scherf, K. Müllen, W. Graupner, C.-H. Kim, J. Shinar, *Phys. Rev. B* 2002, 66, 235203.
- [27] E. J. W. List, C. H. Kim, A. K. Naik, U. Scherf, G. Leising, W. Graupner, J. Shinar, *Phys. Rev. B* 2001, 64, 155204.
- [28] H. Antoniadis, L. J. Rothberg, F. Papadimitrakopoulos, M. Yan, M. E. Galvin, M. A. Abkowitz, *Phys. Rev. B* 1994, 50, 14911.
- [29] M. J. M. de Jong, M. C. J. M. Vissenberg, *Philips J. Res.* 1998, 51, 495.
- [30] C. Schweitzer, R. Schmidt, *Chem. Rev.* 2003, 103, 1685.
- [31] S. Sax, *Diploma Thesis*, Graz University of Technology 2004.
- [32] A. Köhler, J. S. Wilson, R. H. Friend, *Adv. Mater.* 2002, 4, 434.
- [33] M. Reufer, M. J. Walter, P. G. Lagoudakis, A. B. Hummel, J. S. Kolb, H. G. Roskos, U. Scherf, J. M. Lupton, *Nat. Mater.* 2005, 4, 340.
- [34] S. R. Forrest, D. D. C. Bradley, M. E. Thomson, *Adv. Mater.* 2003, 15, 1034.
- [35] S. Gamerith, H.-G. Nothofer, U. Scherf, E. J. W. List, *Jpn. J. Appl. Phys.* 2008, 43, 891.
- [36] S. Kappaun, H. Scheiber, R. Trattnig, E. Zojer, E. J. W. List, C. Slugovc, *Chem. Com.* 2008, 41, 5170.
- [37] M. Schaer, F. Nüesch, D. Berner, W. Leo, L. Zuppiroli, *Adv. Funct. Mater.* 2001, 11, 116.
- [38] N. Koch, *ChemPhysChem* 2007, 10, 1438.
- [39] G. Greczynska, Th. Kuglerb, M. Keila, W. Osikowicza, M. Fahlmann, W.R. Salanecka, *J. Electron. Spectrosc. Relat. Phenom.* 2001, 121, 1.
- [40] U. Scherf, E. J. W. List, *Adv. Mater.* 2002, 14, 477.

- [41] R. Abbel, M. Wolffs, R.A.A. Bovee, J.L.J. van Dongen, X. Lou, O. Henze, W.J. Feast, E.W. Meijer, A.P.H.J. Schenning, *Adv. Mater.* 2009, 21, 597.
- [42] Shimadzu Corp., Instruments handbook SHIMADZU-RF5301PC.
- [43] J. R. Lakowicz, *Principles of Fluorescence Spectroscopy* 3th Edition, 2006 Springer Science + Business Media New York.
- [44] D. Pfeifer, K. Hoffmann, A. Hoffmann, C. Monte, U. Resch-Genger, *J. Fluoresc.* 2006, 16, 581.
- [45] U. Resch-Genger, K. Hoffman, A. Hoffmann, *Ann. N.Y. Acad. Sci.* 2008, 1130, 35.
- [46] Federal Institute of Materials and Testing, Standard operation procedure of 'Spectral fluorescence standard kit'.
- [47] J.A. Gardecki, M. Maroncelli, *Appl. Spectrosc.* 1998, 52, 1179.
- [48] C.A. Parker, W.T. Rees, *Analyst* 1960, 85, 587.
- [49] J. N. Demas, G. A. Crosby, *J. Chem. Phys.* 1971, 75, 991.
- [50] M. Grabolle, M. Spieles, V. Lesnyak, N. Gaponik, A. Eychmuüller, U. Resch-Genger, *Anal. Chem.* 2009, 81, 6285.
- [51] <http://www.horiba.com/us/en/scientific/products/fluorescence-spectroscopy/application-notes/quantum-yields/>, 6.2.2011.
- [52] W.H. Melhuish, *J. Phys. Chem.* 1960, 64, 762.
- [53] <http://en.wikipedia.org/> , 6.02.2011.
- [54] K. Müllen, U. Scherf, *Organic Light Emitting Devices* 1st Edition 2006, Wiley-VCH.
- [55] S. Sax, N. Rugen-Penkalla, A. Neuhold, S. Schuh, E. Zojer, E. J. W. List, K. Müllen, *Adv. Mater.* 2010, 22, 2087.
- [56] W. Zhao, T. Cao, J. M. White, *Adv. Funct. Mater.* 2004, 14, 783.
- [57] S. Kappaun, S. Horner, A.-M. Kelterer, K. Waich, F. Grasse, M. Graf, L. Romaner, F. Niedermair, K. Müllen, A. C. Grimsdale, R. Saf, E. J. W. List, E. Zojer, C. Slugovc, *Macromol. Chem. Phys.* 2008, 209, 2122.
- [58] R. Trattnig, Diploma Thesis, Graz University of Technology, 2009.
- [59] R. D. Scurlock, B. Wang, P. R. Ogilby, J. R. Sheats, R. L. Clough, *J. Am. Chem. Soc.* 1995, 117, 10194.
- [60] M. Jørgensen, K. Norrman, F. C. Krebs, *Sol. Energy Mater. Sol. Cells* 2008, 92, 686.
- [61] A. van Dijken, A. Perro, E.A. Meulenkamp, K. Brunner, *Org. Electron.* 2003, 4, 131.

- [62] C.-Y. Chang, F.-Y. Tsai, S.-J. Jhuo, M.-J. Chen, *Org. Electron.* 2008, 9, 667.
- [63] E. Breitmaier, G. Jung, *Organische Chemie*, Georg Thieme Verlag KG Stuttgart, 2009.
- [64] S. Sax, Dissertation, Graz University of Technology, 2008.
- [65] G. Wurzinger, Diploma Thesis, Graz University of Technology, 2009.
- [66] S. Sax, E. Fisslthaler, S. Kappaun, C. Konrad, K. Waich, T. Mayr, C. Slugovc, I. Klimant, E. J. W. List, *Adv. Mater.* 2009, 21, 3483.
- [67] P. J. Brewer, J. Huang, P. A. Lane, A. J. deMello, D. D. C. Bradley, J. C. de Mello, *Phys. Rev. B* 2006, 74, 115202.
- [68] P. J. Brewer, P. A. Lane, J. Huang, A. J. deMello, D. D. C. Bradley, J. C. de Mello, *Phys. Rev. B* 2005, 71, 205209.
- [69] <http://en.wikipedia.org/wiki/Candela>, 6.02.2011.
- [70] C. L. Gettinger, A. J. Heeger, J. M. Drake, D. J. Pine, *J. Chem. Phys.* 1994, 101, 1673.
- [71] H. H. Fong, J.-K. Lee, Y.-F. Lim, A. A. Zakhidov, W. W. H. Wong, A. B. Holmes, C. K. Ober, G. G. Malliaras, *Adv. Mater.* 2010, 20, 1.